Published in final edited form as:
Cell Rep. 2019 May 14; 27(7): 1979–1990.e7. doi:10.1016/j.celrep.2019.04.084.

Phosphatidylinositol 5 Phosphate 4-Kinase Regulates Plasma-Membrane PIP_3 Turnover and Insulin Signaling

Sanjeev Sharma[1], **Swarna Mathre**[1,2], **Visvanathan Ramya**[1], **Dhananjay Shinde**[1], and **Padinjat Raghu**[1,3,*]

[1]National Centre for Biological Sciences, TIFR-GKVK Campus, Bellary Road, Bangalore 560065, India

[2]Manipal Academy of Higher Education, Manipal, Karnataka 576104, India

Summary

Phosphatidylinositol 3,4,5-trisphosphate (PIP_3) generation at the plasma membrane is a key event during activation of receptor tyrosine kinases such as the insulin receptor required for normal growth and metabolism. We report that in *Drosophila*, phosphatidylinositol 5 phosphate 4-kinase (PIP4K) is required to limit PIP_3 levels during insulin receptor activation. Depletion of PIP4K increases the levels of PIP_3 produced in response to insulin stimulation. We find that PIP4K function at the plasma membrane enhances class I phosphoinositide 3-kinase (PI3K) activity, although the catalytic ability of PIP4K to produce phosphatidylinositol 4,5-bisphosphate [PI(4,5)P_2] at the plasma membrane is dispensable for this regulation. Animals lacking PIP4K show enhanced insulin signaling-dependent phenotypes and are resistant to the metabolic consequences of a high-sugar diet, highlighting the importance of PIP4K in normal metabolism and development. Thus, PIP4Ks are key regulators of receptor tyrosine kinase signaling with implications for growth factor-dependent processes including tumor growth, T cell activation, and metabolism.

Introduction

Lipid kinases phosphorylate selected positions on the inositol head group of phosphatidylinositol (PI) generating second messengers that regulate multiple processes in eukaryotic cells. Phosphatidylinositol 3,4,5-trisphosphate [PI(3,4,5)P_3 or PIP_3] generation from phosphatidylinositol 4,5-bisphosphate [PI(4,5) P_2 or PIP_2] by class I phosphoinositide 3-kinase (PI3K) following growth factor receptor (e.g., insulin receptor) stimulation is a widespread signaling reaction (Hawkins et al., 2006; Vanhaesebroeck et al., 2012) regulating growth and development (Madsen et al., 2018). The role of class I PI3K activation in

*Correspondence: praghu@ncbs.res.in.
[3]Lead Contact

Author Contributions
Conceptualization, P.R. and S.S.; Methodology, P.R., S.S., and D.S.; Investigation, S.S., S.M., and V.R.; Writing, P.R. and S.S.; Funding Acquisition, P.R.

Declaration of Interests
The authors declare no competing interests.

Europe PMC Funders Author Manuscripts

response to insulin receptor signaling is evolutionarily conserved and has been widely studied in metazoans such as the fly, worm, and mammals (Barbieri et al., 2003). Several mechanisms ensure robust control of PIP_3 levels and dynamics. Binding of the class I PI3K heterodimer to p-Tyr residues on adaptor proteins associated with activated receptors relieves the basal inhibition of the regulatory subunit (p85/50/55/60) on the catalytic subunit (p110) (Luo and Cantley, 2005). Additionally, lipid phosphatases including PTEN, a 3-phosphatase, and SHIP2, a 5-phosphatase, can also remove PIP_3 from intracellular membranes (Elong Edimo et al., 2014; Pagliarini et al., 2004). Mutations in genes for any of these enzymes can be oncogenic or result in metabolic syndromes; e.g., loss of PTEN function or gain in class I PI3K activity results in tumor development (Song et al., 2012; Fruman et al., 2017), whereas loss of SHIP2 results in altered insulin sensitivity (Clément et al., 2001). Thus, the control of receptor-activated PIP_3 levels is vital to the regulation of cell growth and metabolism.

PIP_2 (phosphatidylinositol 4,5-bisphosphate), the substrate for PIP_3 production, is mainly synthesized via the phosphorylation of position 5 of the inositol headgroup of phosphatidylinositol 4-phosphate (PI4P) by phosphatidylinositol 4 phosphate 5-kinases (PIP5K) (Stephens et al., 1991). Rameh et al. (1997) later described another class of lipid kinases, the phosphatidylinositol 5 phosphate 4-kinases (PIP4K), that phosphorylate position 4 of phosphatidylinositol 5-phosphate (PI5P) to generate PIP_2. The total cellular PIP_2 mass does not drop upon loss of PIP4Ks, but levels of its preferred substrate, PI5P, are elevated (Gupta et al., 2013; reviewed in Kolay et al., 2016). In mammalian cells, three isoforms of PIP4Ks occur, viz PIP4K2A, PIP4K2B, and PIP4K2C, and vary widely in their *in vitro* enzymatic activity. The mouse knockout phenotypes for each of these genes suggest a role for PIP4Ks in regulating receptor tyrosine kinase and PI3K signaling. Deletions of *PIP4K2A* and *PIP4K2B* slow down tumor growth in $p53^{-/-}$ mice (Emerling et al., 2013); depletion of PIP4K2C results in excessive T cell activation (Shim et al., 2016), and loss of *PIP4K2B* in mice results in hyper-responsiveness to insulin and a progressive loss of body weight in adults (Lamia et al., 2004). Previous studies have linked *PIP4K2B* to insulin and PI3K signaling. Overexpression of PIP4K2B in CHO-IR cells (expressing extremely low levels of endogenous PIP4K2B) reduces insulin-stimulated PIP_3 production (Carricaburu et al., 2003). Similarly, acute doxycycline-induced overexpression of PIP4K2A in U-2 OS cells attenuates insulin-stimulated AKT activation, although PIP_3 levels were not studied under these conditions (Jones et al., 2013). By contrast, a recent study reported that immortalized B cells carrying a deletion of *PIP4K2A* generate reduced levels of PIP_3 following insulin stimulation (Bulley et al., 2016). Thus, multiple lines of evidence link PIP4Ks and class I PI3K signaling during insulin stimulation, although the impact of PIP4K function on PIP_3 levels remains unresolved.

Loss of the only *PIP4K* in *Drosophila* (mutants referred to as $dPIP4K^{29}$) results in a larval growth deficit and developmental delay associated with an overall reduction in the levels of $pS6K^{T398}$ and $pAKT^{S505}$, both outputs of mechanistic target of rapamycin (mTOR) signaling. Enhancing mTOR complex 1 (TORC1) activity through pan-larval overexpression of its activator Rheb rescues the systemic growth defect in $dPIP4K^{29}$ (Durán and Hall, 2012; Gupta et al., 2013). Since then, PIP4K2C has also been shown to regulate TORC1-mediated signaling in immune cells, and PIP4K2C enhances TORC1 outputs in Tsc1/2-depleted cells

during starvation (Mackey et al., 2014). mTOR signaling transduces multiple developmental and environmental cues like growth factor signaling, amino acid levels, and cellular ATP levels into growth responses (Wullschleger et al., 2006). However, the relationship between PIP4K function, its role in regulating TORC1 activity, and class I PI3K signaling remains unclear.

During *Drosophila* larval development, a dramatic increase in body size occurs without increases in cell number but via an increase in cellular biomass of polyploid larval tissues such as the salivary gland and fat body (Church and Robertson, 1966). This form of growth is driven by ongoing insulin signaling mediated through the endocrine secretion of *Drosophila* insulin-like peptides (dILPs) from insulin-producing cells (IPCs) in the larval brain and their action on peripheral tissues through the single insulin receptor (Brogiolo et al., 2001). Removal of the insulin receptor (*dInR*) (Shingleton et al., 2005) or the insulin receptor substrate (*chico*) (Böhni et al., 1999) reduces growth and delays development through multiple mechanisms. In flies, salivary gland cell size can be tuned by enhancing cell-specific class I PI3K-dependent PIP_3 production (Georgiev et al., 2010). In this study, we use salivary glands and fat body cells of *Drosophila* larvae to study the effect of dPIP4K on insulin receptor-activated class I PI3K signaling. We find that loss of *dPIP4K* leads to a cell-autonomous increase in the levels of basal and insulin-stimulated PIP_3. dPIP4K acts at the plasma membrane to regulate the levels of PIP_3 by modulating the class I PI3K activity. Moreover, the growth-promoting effects of the insulin signaling pathway are enhanced in the absence of dPIP4K. Finally, these cellular changes in insulin signaling have consequences on circulating sugar metabolism in larvae and alter their susceptibility to acquiring insulin resistance on a high-sugar diet (HSD). Altogether, we demonstrate dPIP4K as a physiologically important negative regulator of class I PI3K signaling during *Drosophila* insulin stimulation *in vivo*.

Results

Loss of PIP4K Elevates PIP_3 Levels in *Drosophila* Cells

Plasma membrane PIP_3 production upon class I PI3K activation is an essential early event during receptor tyrosine kinase signaling (Auger et al., 1989; Hawkins et al., 2006; Kelly and Ruderman, 1993). We employed two methods to measure PIP_3 levels from *Drosophila* larvae. First, we estimated PIP_3 levels at the plasma membrane of individual cells by imaging salivary glands and fat body lobes of wandering third instar larvae expressing a PIP_3-specific probe (GFP::PH-GRP1) (Britton et al., 2002). Salivary glands and fat body are organs composed of large insulin-responsive cells amenable to microscopy and *ex vivo* manipulations. Under basal conditions, the plasma membrane PIP_3 in $dPIP4K^{29}$ salivary glands, as well as fat body cells, showed a small but significant elevation compared with wild type (Figures 1Ai, 1Aii, 1Bi, and 1Bii). In an alternative approach, we quantified total PIP_3 mass in whole larval lipid extracts using liquid chromatography coupled with mass spectrometry (LCMS) (see also STAR Methods and Figures S1D–S1F). Unlike the single-cell PIP_3 estimates from salivary glands and fat body cells, there was no significant difference in the total PIP_3 levels measured using LCMS from wild-type and $dPIP4K^{29}$ larvae (Figure 1C). Thus, the loss of dPIP4K leads to a basal elevation of PIP_3 levels in cells,

although total organismal PIP_3 mass does not reflect the same, likely because of the heterogeneous effects of dPIP4K depletion in individual larval tissues.

During larval development in *Drosophila*, nutritional and developmental cues elicit the endocrine release of dILPs (Nässel and Vanden Broeck, 2016), which activate dInR triggering class I PI3K activation and PIP_3 production. Therefore, the elevated PIP_3 levels observed in $dPIP4K^{29}$ tissues could result from: (1) enhanced production and release of dILPs, (2) upregulation in insulin receptor levels, and (3) increase in insulin receptor activity or events downstream of receptor activation. To distinguish between these possibilities, we measured mRNA levels of *dILP2, 3, 5* (known to be transcriptionally regulated) (Brogiolo et al., 2001) and found them relatively unchanged in $dPIP4K^{29}$ (Figure S1A). dILP2 immunoreactivity in the IPCs of the larval brain is indicative of the status of dILP release and is expected to be lower when more dILP2 is released into the hemolymph. Immunostaining of dILP2 in the IPCs was not lower in $dPIP4K^{29}$ compared with controls (Figures S1Bi and S1Bii), indicating that $dPIP4K^{29}$ larvae did not have enhanced levels of hemolymph dILP2. Further, *dInR* receptor mRNA levels in $dPIP4K^{29}$ were comparable with wild type, indicating that the levels of dInR activated by dILPs were also unlikely to be different between the two genotypes (Figure S1C). Collectively, we observed elevated PIP_3 levels in cells lacking dPIP4K without evidence of increased humoral dILP secretion or insulin receptor levels.

Because the differences in PIP_3 levels between $dPIP4K^{29}$ and control larvae were modest under basal conditions, we used an *ex vivo* assay to study the role of dPIP4K in cells during insulin stimulation. *Drosophila* cells respond to bovine insulin using signal transduction elements that are conserved with the canonical mammalian insulin signaling pathway (Lizcano et al., 2003). Imaging GFP::PH-GRP1 probe in salivary glands and fat body dissected from third instar larvae confirmed that *ex vivo* bovine insulin stimulation triggered a rise in plasma membrane PIP_3 levels. Interestingly, insulin-stimulated (10 min, 10 μM) PIP_3 levels in $dPIP4K^{29}$ were higher than in wild type (Figures 1Di and 1Dii). Also, the difference in PIP_3 levels between $dPIP4K^{29}$ and controls following insulin stimulation was noticeably greater than observed under basal conditions (compare Figures 1Aii and 1Dii). Similarly, in fat body cells, PIP_3 production increased over a 100-fold range of insulin concentrations. Whereas 100 nM insulin barely elicited an increase in PIP_3 levels, we found fat body cells of $dPIP4K^{29}$ showed a larger rise in PIP_3 levels compared with controls at higher concentrations of insulin (Figures 1Ei–1Eiii). Further, total PIP_3 mass analyzed from whole larval lipid extracts of insulin-stimulated larvae revealed that $dPIP4K^{29}$ larvae had significantly higher PIP_3 levels than wild type (Figures 1F and S2B). Thus, the modest elevation in the basal PIP_3 levels seen in the absence of dPIP4K was further enhanced by *ex vivo* insulin stimulation.

Cell-Autonomous Control of Plasma Membrane PIP_3 Levels by dPIP4K

Because humoral dILP signals were not higher in $dPIP4K^{29}$, we tested whether the elevated PIP_3 levels in $dPIP4K^{29}$ larvae resulted from cell-autonomous changes in salivary gland cells. Reconstituting dPIP4K specifically in salivary glands of $dPIP4K^{29}$ larvae ($AB1{>}dPIP4K^{WT}; dPIP4K^{29}$) resulted in a reduction of plasma membrane PIP_3 levels

(Figure 2A). Further, we tested whether regulation of PIP_3 levels by dPIP4K required its kinase activity by reconstituting a kinase-dead enzyme in *dPIP4K*^{29}. A point mutation, D271A, in dPIP4K abolishes its kinase activity (Figures S2D and S2E, referred to as *dPIP4K*^{KinaseDead} hereafter). *dPIP4K*^{KinaseDead} rescued the elevated PIP_3 levels back to those seen in controls (Figure 2B). Salivary gland-specific depletion of dPIP4K (*AB1>; dPIP4K*^{RNAi}) (Figure 2Ci) also increased insulin-stimulated PIP_3 levels compared with controls (Figure 2Cii).

Likewise, PIP_3 levels were also elevated in *Drosophila* $S2R^+$ cells where dPIP4K was depleted using double-stranded RNA (dsRNA) treatment (also reflected in the levels of all of the individual species) (Figures 2Di, 2Dii, and S2C). Downstream effects of PIP_3 signaling such as the $pAKT^{T342}$ levels (the equivalent of mammalian $pAKT^{T308}$ and phosphorylated by phosphoinositide-dependent kinase [PDK1]; Alessi et al., 1997) and $p\text{-}S6K^{T398}$, a target of TORC1, were also elevated in dPIP4K-depleted cells (Figures 2Ei and 2Eii). Together, these observations suggest a cell-autonomous role for dPIP4K, independent of its ability to produce $PI(4,5)P_2$, in limiting the levels of PIP_3 and its downstream signaling during insulin stimulation.

PIP4K Functions at the Plasma Membrane to Regulate Insulin-Stimulated PIP_3 Signaling

We and others have seen PIP4Ks localize to multiple subcellular compartments (Clarke et al., 2010; Gupta et al., 2013). The substrate for PIP4K (i.e., PI5P) is also reported to occur on various organelle membranes (Sarkes and Rameh, 2010). We sought to understand the sub-cellular compartment from which dPIP4K regulates plasma membrane PIP_3 levels. We first established that the reduced TORC1 activity reported earlier in *dPIP4K*^{29} mutants (Gupta et al., 2013) did not drive the increase in PIP_3 levels because of a loss of negative feedback activity (Figure S3). Next, we used unique signal sequences (Figure 3A) to selectively target dPIP4K to distinct compartments including lysosomes, endomembranes, viz the endoplasmic reticulum (ER) and Golgi, and the plasma membrane (Figures 3Bi–3Biv, compare localizations with the wild-type enzyme), and confirmed them to be enzymatically active (Figures 3Ci and 3Cii). We then used salivary gland-specific reconstitution to test the ability of these constructs to revert the enhanced insulin-stimulated PIP_3 production in *dPIP4K*^{29}. Under these conditions, only the plasma membrane-targeted dPIP4K completely restored the elevated PIP_3 levels in *dPIP4K*^{29} to that of controls (Figure 3F), whereas the lysosome-targeted (Figure 3D) and endomembrane dPIP4K (Figure 3E) failed to do so. Overexpression of plasma-membrane-targeted dPIP4K in wild-type salivary glands phenocopies overexpression of wild-type dPIP4K in suppressing insulin-stimulated PIP_3 levels (Figure 3G).

We compared the effect of overexpressing a human PIP4K2B with a CAAX-motif at its C terminus that localizes it to the plasma membrane against wild-type PIP4K2B in CHO-IR cells (compare localizations in Figure 3Hi). In these cells, overexpression of PIP4K2B reduces the levels of $pAKT^{T308}$, a downstream effect of PIP_3-dependent signaling during insulin stimulation (Carricaburu et al., 2003). Consistent with our findings in *Drosophila* cells, serum-starved CHO-IR cells transiently overexpressing either PIP4K2B::eGFP or $PIP4K2B::mCherry^{CAAX}$ showed a small but significant reduction in $pAKT^{T308}$ levels upon

insulin stimulation (Figure 3Hii). In fact, this decrease was achieved for PIP4K2B::mCherry^{CAAX} despite much lower levels of expression compared with the wild-type protein. Thus, our results suggest that plasma-membrane-localized PIP4K is sufficient to limit PIP_3 levels and downstream signaling during insulin stimulation.

dPIP4K Alters PIP_3 Turnover by Limiting Class I PI3K Activity

To observe real-time PIP_3 dynamics upon insulin stimulation, we developed a live-imaging assay using the GFP::PH-GRP1 probe in salivary gland cells. Key reactions involved in this process and the assay protocol are depicted in Figures 4Ai and 4Aii, respectively. The dynamics of PIP_3 turnover show three phases: (1) insulin-stimulated increase in PIP_3 levels upon PI3K activation with relatively lower phosphatase activity (rise); (2) PIP_3 levels achieve a steady state as the opposing kinase and phosphatase activities balance each other (steady state); and (3) wortmannin inactivates PI3K, whereas phosphatases remain active, leading to a fall in PIP_3 levels (decay) (Figure 4Bi). Class I PI3K inhibition was effective and specific as wortmannin abolished insulin-stimulated PIP_3 production in contrast with addition of just the vehicle (DMSO) (Figures 4Bii and 4Biii).

Using this assay, we observed that loss of dPIP4K resulted in higher steady-state levels of PIP_3 in salivary gland cells compared with controls (Figure 4C), and overexpression of dPIP4K (Figure 4D) resulted in lower steady-state levels of PIP_3, consistent with our earlier results from fixed salivary glands (Figures 1Dii and 3G). Analysis of the rate of change in PIP_3 levels during the initial rise phase clearly revealed enhanced PIP_3 production rates in *dPIP4K*^{29} following insulin stimulation and conversely reduced rates of PIP_3 production upon overexpression of dPIP4K (Figure 4Ei). In a similar analysis of the decay phase (i.e., upon class I PI3K inactivation), the rate of decay in PIP_3 levels was marginally slower in dPIP4K-depleted cells and even slower in dPIP4K-overexpressing cells relative to controls (Figure 4Eii). Initial studies with fixed insulin-stimulated salivary glands expressing the GFP::PH-GRP1 probe had failed to reveal these differences (Figures S5Bi and S5Bii). When the directions of changes in steady-state PIP_3 levels and the enzyme activities are considered together, our findings imply that dPIP4K modulates the activity of both the kinases and phosphatases involved in PIP_3 turnover, but appears to have a significantly greater effect on class I PI3K activity.

Loss of dPIP4K Enhances Physiological Outputs of Insulin Signaling *In Vivo*

Insulin-stimulated production of PIP_3 is closely linked to its downstream effects on cell physiology (Kelly and Ruderman, 1993). We used salivary glands as a model organ to study changes in cell size (Georgiev et al., 2010; Gupta et al., 2013) and sought to establish if the elevated PIP_3 resulting from loss of dPIP4K impacts insulin signaling-dependent cell physiology. Insulin receptor signaling can autonomously control both cell size and proliferation (Figure 5A) (Böhni et al., 1999; Brogiolo et al., 2001), although direct evidence for such regulation in salivary glands has not been reported. In proof of principle experiments, salivary gland-specific depletion of insulin receptor (*dInR*) levels through RNAi (*AB1>InR*^{RNAi}) reduced the average size of salivary gland cells without changing the number of cells (Figures 5B and 5C). Conversely, dInR and Chico overexpression (Figures

5Di and 5Ei) increased the average cell size, confirming the role of insulin signaling in regulating salivary gland cell size.

Next, we compared the effect of overexpressing insulin signaling components on wild-type and *dPIP4K*^{29} salivary gland cells. Both *dInR* (Figures 5Di and 5Dii) and insulin receptor substrate, *Chico* (Figures 5Ei and 5Eii), increased salivary gland cell size in wild type and *dPIP4K*^{29}. However, in both manipulations the increase in cell size elicited was significantly greater in *dPIP4K*^{29} (*AB1>dInR* [or *Chico*]*; dPIP4K29*) compared with wild-type cells (*AB1>dInR* [or *Chico*]) (Figure 5G). If PIP4K acted at the plasma membrane to limit PIP_3 production *in vivo*, constitutively activating a component downstream of PIP_3 synthesis would be expected to abolish the differences between wildtype and *dPIP4K*^{29} cells. As predicted, unlike the *dInR* and *Chico* manipulations, expression of a constitutively active form of phosphoinositide-dependent kinase-1 (*PDK1*)-PDK1^{A467V}, normally activated by PIP_3-binding during insulin receptor activation (Paradis et al., 1999; Rintelen et al., 2001), resulted in an equivalent cell size increase in wild-type and *dPIP4K*^{29} salivary glands (Figures 5Fi, 5Fii, and 5G).

If the insulin signaling pathway is indeed modulated by dPIP4K, it is expected to alter the physiological response of the animals to sugar intake. Larvae raised on a HSD have reduced body weight, developmental delay, and elevated levels of trehalose, the main circulating sugar in insect hemolymph. These phenotypes are reminiscent and equivalent to the development of insulin resistance in type II diabetes (Musselman et al., 2011; Pasco and Léopold, 2012). Using this paradigm (Figure S6A), we found that wild-type larvae showed a delay in development (ca. of 9 days) when grown on HSD (1 M sucrose) through larval development, compared with animals grown on normal food (0.1 M sucrose), as seen by the time taken by a population of larvae to pupariate. Interestingly, *dPIP4K*^{29} larvae grown on HSD were retarded to a much lesser magnitude (delay of only 5 days) compared with their growth on 0.1 M sucrose (Figure S6B). The levels of circulating trehalose in the hemolymph of wandering third instar larvae of *dPIP4K*^{29} raised on normal food were ca. 40% lower compared with controls. But on HSD, while in the wild-type larvae, the circulating trehalose level had risen by ca. 25% compared to ND, in *dPIP4K*^{29}, it essentially remained unchanged (Figure S6C).

Further, we modified and developed a shorter growth analysis protocol to test the requirement of the kinase activity of dPIP4K in the regulation of sugar metabolism. Here, larvae were exposed to the HSD only during the latter part of the third instar stage (depicted in Figure S6D). Under these conditions, control animals (*Act>*) showed a delay of ca. 65 h when grown on HSD compared with those on normal food (Figure 5H), whereas HSD-induced delay in *dPIP4K*^{29} (*Act>; dPIP4K*^{29}) was only ca. 56 h (Figure 5J). We then compared the ability of the wild-type and kinase-dead dPIP4K to revert the HSD-induced delay in *dPIP4K*^{29} to those seen in control larvae. Only the wild-type *dPIP4K* transgene (*Act>dPIP4K*^{WT}*;dPIP4K*^{29}) (Figure 5I) restored the delay induced by HSD close to that seen in control animals, i.e., ca. 63 h, whereas the *kinase-dead* transgene (*Act>dPIP4K*^{KinaseDead}*; dPIP4K*^{29}) was incapable of doing so, and the delay was similar to that seen in *dPIP4K*^{29} (Figure 5K). This indicates a role for the kinase activity of dPIP4K in supporting organismal control of sugar metabolism. Also, collectively our observations

suggest that loss of dPIP4K modulates insulin receptor signaling *in vivo* and can confer partial protection against HSD-induced phenotypes.

Discussion

The core enzymes directly involved in PIP_3 metabolism, a highly conserved element of signal transduction through many growth factor receptors, have been extensively studied. However, factors regulating their activity remain less understood. Some small GTPases (Ras, Rac) and $G_{\beta\gamma}$ subunits are shown to be involved in the regulation of class I PI3K activity (reviewed in Hawkins and Stephens, 2015). Our study identifies *dPIP4K* as a negative regulator of PIP_3 levels during growth factor stimulation. This is evident from the elevated insulin-stimulated PIP_3 levels seen in the mutants for the only PIP4K gene in *Drosophila* (Balakrishnan et al., 2015; Gupta et al., 2013). Further, we have demonstrated that this function of dPIP4K is cell autonomous by negating a role for the humoral signals that impinge on insulin signaling and also by altering PIP_3 levels through tissue-specific manipulations of dPIP4K in salivary glands and in dPIP4K-depleted *Drosophila* $S2R^+$ cells. Many direct and indirect mechanisms have been proposed to regulate PIP_3 levels. In an earlier study (Gupta et al., 2013), it was reported that $dPIP4K^{29}$ larvae have reduced mTORC1 activity. Thus, a loss of TORC1-mediated feedback control on insulin receptor signaling, as demonstrated to occur in mammalian cells (Gual et al., 2005; Haruta et al., 2000; O'Reilly et al., 2006; Tremblay et al., 2007; Um et al., 2004), may be the underlying reason for increased PIP_3 levels in $dPIP4K^{29}$. However, we ruled out this possibility by demon-strating that enhancing TORC1 activity was not able to revert elevated PIP_3 levels in $dPIP4K^{29}$ salivary gland cells despite causing expected changes in cell size (Figures S3A–S3G). Our data clearly demonstrate that both TORC1 and dPIP4K are required to limit PIP_3 levels in cells during insulin signaling.

In contrast with our previous study, where mTOR signaling read-outs like $pS6K^{T398}$ and $pAKT^{s505}$ levels were reduced in whole larval extracts of $dPIP4K^{29}$ (Gupta et al., 2013), depleting dPIP4K in $S2R^+$ cells led to a cell-autonomous increase in mTOR signaling downstream of insulin stimulation as seen by increased $pAKT^{T342}$ as well as $pS6K^{T398}$ levels (Figure 2Eii). The discrepancy between the two observations is likely due to variable levels of TORC1 activation in various larval tissues and cell types in $dPIP4K^{29}$ (data not shown). mTOR activity is determined by multiple humoral signals in the context of a whole organism that may or may not require dPIP4K function in specific tissues (Colombani et al., 2003; Géminard et al., 2009). Our inability to observe an increase in basal PIP_3 levels from whole larvae also hints toward this possibility.

Although PIP4K and its substrate, PI5P, occur on multiple sub-cellular compartments (Clarke et al., 2010; Gupta et al., 2013; Sarkes and Rameh, 2010), we found that the plasma membrane-localized pool of PIP4K is sufficient to regulate PIP_3 levels in cells from two different species: first in *Drosophila* cells, by rescuing elevated PIP_3 levels in $dPIP4K^{29}$ by selective reconstitution with the plasma membrane-targeted enzyme; and second, in mammalian cells, by demonstrating a reduction in $pAKT^{308}$ phosphorylation by overexpression of plasma membrane-localized PIP4K2B just as well as with wild-type PIP4K2B. These observations point to the evolutionarily conserved nature of this

Europe PMC Funders Author Manuscripts

mechanism and are also consistent with a role for PIP4K in direct regulation of PIP_3 independent of TORC1-mediated feedback control. Our live-imaging studies using chemical inhibition of class I PI3K also suggest that dPIP4K acts majorly by limiting the class I PI3K activity to regulate PIP_3 levels with a marginal effect on the phosphatases. However, the exact mechanism by which it does so remains to be established.

Loss of PIP4K results in an elevation rather than a reduction in PIP_3 levels, and a kinase-dead version of dPIP4K was also able to reduce PIP_3 levels, which implies that the conversion of PI5P to $PI(4,5)P_2$ by dPIP4K is not required to support the PIP_3 production by class I PI3K. In addition to PIP_3, we also measured the levels of PIP_2, the substrate of class I PI3K for PIP_3 production, using LCMS and live imaging of the PIP_2-probe (PH-PLCδ::mCherry). Prior to insulin stimulation, resting PIP_2 levels from larval tissues of *dPIP4K*^{29} were no different from that of controls (Figure S5Bi). However, unlike wild-type cells where insulin stimulation did not change PIP_2 levels (Figures S5Bii and S5Di), in dPIP4K-depleted cells, PIP_2 levels rose substantially along with PIP_3 levels (Figures S5Bii and S5Dii and trends observed in Figure S5C, although not statistically significant). These findings imply that during class I PI3K signaling, normal PIP4K function is also required to regulate PIP_2 levels at the plasma membrane. It is unclear if the elevated PIP_2 levels seen during insulin signaling directly underlie the elevated PIP_3 levels in PIP4K-depleted cells. This seems unlikely because in almost all cell types and organisms studied so far, PIP_2 levels are at least 500-fold more than PIP_3 levels (recent example of PIP_2 and PIP_3 levels measured in mammalian cells; Malek et al., 2017), and therefore an active mechanism must exist to ensure generation of only a small amount of PIP_3 from a much larger fraction of readily available PIP_2. Moreover, PIP4K-depleted cells do not possess elevated basal levels of PIP_2, which might support increased PIP_3 production during stimulation. However, a link between the levels of the two lipids cannot be ruled out completely. Interestingly, a recent study has reported that cells depleted of PIP4K show elevated levels of PIP2 and PIP3; evidence is presented that the interaction of PIP5K, the enzyme that synthesizes the majority of PIP2 cells, is inhibited by its interaction with PIP4K (Wang et al., 2019).

Alternatively, elevated PI5P levels reported in PIP4K-depleted cells might mediate the increase in PIP_3 levels by promoting class I PI3K activity. Previous studies have shown that levels of PI5P increase upon insulin stimulation and importantly, addition of exogenous PI5P can stimulate glucose uptake in a PI3K-dependent manner (Grainger et al., 2011; Jones et al., 2013). In PIP4K-depleted cells, PI5P levels could rise unchecked at the plasma membrane during insulin stimulation, resulting in higher levels of PIP_3. This model appears inconsistent with the tissue-specific rescue of elevated PIP_3 levels in PIP4K-depleted cells by dPIP4K^{KinaseDead}, which cannot produce PIP_2 from PI5P because of its inability to hydrolyze ATP. However, when highly expressed (Figure S2F), such a rescue could simply occur through binding and sequestration of PI5P by dPIP4K^{KinaseDead}. Identification and generation of a PI5P-binding mutant of PIP4K will be required to test this model. Interestingly, pan-larval expression of *dPIP4K*^{KinaseDead} was unable to rescue the impact of dPIP4K depletion on the growth of larvae grown on HSD, whereas only the wild-type transgene could. This agrees with a recent study where the requirement of dPIP4K in regulating salivary gland cell size was seen to depend on the kinase activity of the enzyme (Mathre et al., 2019). Future *in vivo* studies would require precise control of the expression

and analysis of multiple tissues to clearly delineate kinase-dependent and -independent roles for PIP4K.

Elevated PIP_3 levels, altered PI3K activity, and TORC1 activation in cells lacking dPIP4K would predict important physiological consequences on cell growth and sugar metabolism *in vivo*. Consistent with the idea of being a negative regulator, absence of dPIP4K enhanced the growth-promoting ability of insulin signaling components. Using a high-sugar-induced obesity and type II diabetes-like insulin resistance model (Musselman et al., 2011), we found that $dPIP4K^{29}$ larvae appear partially resistant to the effects of a HSD, such as changes in hemolymph trehalose levels and developmental delay. These observations are reminiscent of phenotypes for PIP4K2B$^{-/-}$ mice that also have a reduced adult body weight and clear blood glucose faster following a sugar bolus than controls (Lamia et al., 2004). Our observation that dPIP4K controls sensitivity to insulin receptor activation at the plasma membrane suggests a molecular basis for the physiological phenotypes observed in $dPIP4K^{29}$ larvae and PIP4K2B$^{-/-}$ mice. Such a mechanism may also explain the hyperactivation of the T cell receptor responses in mice lacking PIP4K2C (Shim et al., 2016), because the activation of class I PI3K is a key element of T cell receptor signal transduction. More generally, modulation of PIP4K function offers a mechanism to precisely regulate class I PI3K activity in the context of receptor tyrosine kinase signaling.

Star★Methods

Key Resources Table

REAGENT or RESOURCE	SOURCE	IDENTIFIER
Antibodies		
Rabbit polyclonal anti- α-actin	Sigma Aldrich	A5060; RRID: AB_476738
Rabbit polyclonal anti- dPIP4K	Generated for the lab by NeoBiolab (NeoScientific, Cambridge, MA)	N/A
Rabbit polyclonal anti-GAPDH	Novus Biologicals	IM-5143A; RRID: AB_1150416
Rabbit polyclonal anti-PIP4KB	Cell Signaling Technology	9694; RRID: AB_2164572
Rabbit polyclonal anti – pAKT (T308)	Cell Signaling Technology	9275; RRID: AB_329828
Rabbit polyclonal anti-AKT	Cell Signaling Technology	9272; RRID: AB_329827
Rabbit polyclonal anti-pS6K (T398)	Cell Signaling Technology	9209: RRID: AB_2269804
Rabbit polyclonal anti-pAKT1 (T342)	Abcam	ab228808
Rabbit polyclonal dILP2 antibody	Gift from Prof. Jan Veenstra, INCI, Uni. Of Bordeaux	N/A
Chemicals		
Drosophila Schneider’s medium	GIBCO	21720024
Drosophila Schneider’s medium	Himedia Labs.	IML003A
Fetal Bovine Serum	GIBCO	16000044
Bovine Insulin	SIGMA	I6634
Penicilllin-Streptomycin-Glutamine Mix	SIGMA	G1146
	Himedia Labs.	A007

REAGENT or RESOURCE	SOURCE	IDENTIFIER
Megascript RNAi Kit	AMBION, Life Technologies	AM1626
Porcine Trehalase	SIGMA	T8778
G418	Himedia Labs.	TC025
BODIPY® FL C12-Sphingomyelin	Life Technologies	D-7711
Fugene® 6	Promega Corporation	E2692
Effectene	QIAGEN	301425
17:0 20:4 PI(3,4,5)P3	Avanti Polar Lipids	LM 1906
Glucose (GO) Assay Kit	SIGMA	GAGO-20
Experimental Models: Cell Lines		
CHO-IRA	Gift from Prof. Nicholas Webster,UCSD	N/A
S2R+ - ActGal4	Gift from Satyajit Mayor Lab, NCBS.	N/A
Experimental Models: Organisms/Strains		
Red Oregon R (ROR) - wildtype	Bloomington	2376
AB1-Gal4	Bloomington	1824
UAS-dInR	Bloomington	8262
UAS-Rheb	Bloomington	9688
UAS-Rheb^{RNAi}	Bloomington	33966
UAS-TSC^{RNAi}	Bloomington	52931
P{tGPH}4	Bloomington	8164
UAS-dPIP4K^{RNAi}	Bloomington	65891
Act5cGal4	Bloomington	3953
UAS-4cPH-PLCδ1::mCherry	Patrick Verstreken, VIB, Belgium.	N/A
dPIP4K29	Lab generated	N/A
UAS-dPIP4K^{wt}	Lab generated	N/A
UAS-dPIP4K^{KinaseDead}	Lab generated	N/A
UAS-dPIP4K::eGFP	Lab generated	N/A
UAS-dPIP4K::-mCherry-CAAX	Lab generated	N/A
UAS-Lysosomal-dPIP4K::eGFP	Lab generated	N/A
UAS-Endomembrane-dPIP4K::mCherry	Lab generated	N/A
Oligonucleotides		
Ctrl (GFP)_dsRNA_Fwd	TAATACGACTCACTATAGGGATGG TGAGCAAGGGCGAGGAG	Ctrl (GFP)_dsRNA_Fwd
Ctrl (GFP)_dsRNA_Rev	TAATACGACTCACTATAGGGCTTG TACAGCTCGTCCATGCCG	Ctrl (GFP)_dsRNA_Rev
PIP4K dsRNA I F (DRSC17213)	TAATACGACTCACTATAGGGAAGTTTGA TTTAAAAGGTAGCAC	PIP4K dsRNA I F (DRSC17213)
PIP4K dsRNA I R (DRSC17213)	TAATACGACTCACTATAGGGCTCAGCG TGTCCATTAGTTT	PIP4K dsRNA I R (DRSC17213)
PIP4K dsRNA II F (DRSC39291)	TAATACGACTCACTATAGGGAAACA TGCCGTCACATTTCA	PIP4K dsRNA II F (DRSC39291)
PIP4K dsRNA II R (DRSC39291)	TAATACGACTCACTATAGGGGAGG TAACAGCGTTTTTCCG	PIP4K dsRNA II R (DRSC39291)

REAGENT or RESOURCE	SOURCE	IDENTIFIER
Software and Algorithms		
Volocity	Perkin Elmer Inc.	Ver 5.5.1
MultiQuant	AB SCIEX	Ver 1.1

Contact for Reagent and Resource Sharing

Further information and requests for resources and reagents should be directed to and will be fulfilled by the Lead Contact, Raghu Padinjat (praghu@ncbs.res.in).

Experimental Model and Subject Details

***Drosophila* strains and rearing—**Unless indicated, flies were grown on standard fly medium containing corn meal, yeast extract, sucrose, glucose, agar and antifungal agents. For all experiments, crosses were setup at 25°C in vials/bottles under non-crowded conditions. The stocks that were used in the study are described in the table of key resources. The fly media used had the following composition:

Ingredients	0.1 M sucrose	1 M sucrose
For 1 Liter		
Corn flour	80 g	80 g
D-Glucose	20 g	20 g
Sugar	40 g	342 g
Agar	8 g(4g)	8 g
Yeast powder	15 g	15 g
Propionic acid	4 ml	4 ml
TEGO(Methyl parahydroxy benzoate)	0.7 g	0.7 g
Orthophosphoric acid	0.6 ml	0.6 ml

Genotypes represented across figures—Figure 1 - A, B, D and E. *tGPH* and *tGPH; dPIP4K^{29}*. C and F. *ROR* and *dPIP4K^{29}*.

Figure 2 - A. AB1Gal4, tGPH/+; dPIP4K^{29} and UAS-dPIP4K^{WT}/+; AB1Gal4, tGPH/+; dPIP4K^{29} B. AB1Gal4, tGPH/+, AB1Gal4, tGPH/+; dPIP4K^{29} and UAS-dPIP4K^{KinaseDead}/+; AB1Gal4, tGPH/+; dPIP4K^{29}. C. AB1Gal4, tGPH/+ and UAS-dPIP4K^{RNAi}/+; AB1Gal4, tGPH/+.

Figure 3 - D. AB1Gal4, tGPH /+ and AB1Gal4, tGPH /+; dPIP4K^{29} and AB1Gal4, tGPH / Lysosomal-dPIP4K::eGFP; dPIP4K^{29}. E. AB1Gal4, tGPH /+ and AB1Gal4, tGPH /+; dPIP4K^{29} and AB1Gal4, tGPH /dPIP4K::mCherryEM; dPIP4K^{29}. F. AB1Gal4, tGPH /+ and

AB1Gal4, tGPH /+; dPIP4K^{29} and AB1Gal4, tGPH /dPIP4K::mCherryCAAX; dPIP4K^{29}. G. AB1Gal4, tGPH /+ and UAS-dPIP4K^{WT} /+; AB1Gal4, tGPH /+ and AB1Gal4, tGPH / UAS-dPIP4K::mCherry^{CAAX}.

Figure 4 - B(i-iii). AB1Gal4, tGPH/+. C. AB1Gal4, tGPH/+ and AB1Gal4, tGPH/+; dPIP4K^{29}. D. AB1Gal4, tGPH/+ and UAS-dPIP4K^{WT}/+; AB1Gal4, tGPH/+. FG. AB1Gal4, tGPH/+ and UAS-dPIP4K^{RNAi}/+; AB1Gal4, tGPH/+.

Figure 5 - B, C. AB1Gal4/+ and AB1Gal4; UAS-dINR^{RNAi}. D(i). AB1Gal4/+ and UAS-dINR/+; AB1Gal4/+ and (ii). AB1Gal4/+; dPIP4K^{29} and UAS-dINR/+; AB1Gal4/+; dPIP4K^{29}. E(i). AB1Gal4/+ and UAS-Chico/+; AB1Gal4/+ and (ii). AB1Gal4/+; dPIP4K^{29} and UAS-Chico/+; AB1Gal4/+; dPIP4K^{29}. F(i). AB1Gal4/+ and UAS-PDK1^{A467V}/+; AB1Gal4/+ and (ii). AB1Gal4/+; dPIP4K^{29} and UAS-PDK1^{A467V}/+; AB1Gal4/+; dPIP4K^{29}. H. Act5cGal4/+. I. Act5CGal4/+; UAS-dPIP4K; dPIP4K^{29}. J. Act5CGal4/+; dPIP4K^{29}. K. Act5CGal4/+; UAS- dPIP4K^{KinaseDead}; dPIP4K^{29}.

Method Details

DNA constructs and transgenic flies—For PIP_3 measurements in the *dPIP4K^{29}* rescue experiment (Figure 2A) using GFP-PH-GRP1 probe, we cloned dPIP4K cDNA (BDGP clone# LD10864) into pUAST-attB between EcoRI and *XhoI* sites without any tag. The generation of flies expressing dPIP4K::mCherry-CAAX was first described in (Kamalesh et al., 2017). Briefly, we amplified the mCherry-CAAX fragment from pcDNA3-mCherry-CAAX. We used GIBSON assembly to insert the mCherry–CAAX sequence at the C-terminal of PIP4K after a flexible linker sequence (GGSGGGSGGGSG) by introducing overlaps during the PCR step. Similarly, for targeting dPIP4K to the endomembranes, the sequence QGSMGLPCVVM (Sato et al., 2006) replaced the CAAX motif in the dPIP4K::mCherry-CAAX construct. To generate Lysosomal-dPIP4K::eGFP, the 39 amino-acid sequence from p18/LAMTOR (Menon et al., 2014) was used as a signal sequence. The signal sequence was commercially synthesized with a C-terminal flag tag and introduced upstream of dPIP4K::eGFP. The entire fusion construct was cloned into pUAST-attB by GIBSON assembly using *NotI* and *XbaI* sites. The constructs were transfected in S2R+ cells using Effectene as per manufacturer's protocol and their localization was confirmed by imaging using a 60X objective on a Olympus FV 3000 confocal microscope. Site-directed mutation to generate kinase dead dPIP4K (Aspartic acid at position 271 mutated to Alanine) was introduced through PCR amplification of the plasmid containing the wild-type untagged dPIP4K gene, using primers containing the desired mutation in the middle flanked on either side by exactly complementary nucleotides. All molecular constructs were conceptualized and analyzed further with use of the molecular cloning tools available on the free online platform – Benchling.com. The transgenic lines were generated by site-specific recombination in transgenic parent lines containing attP sites. It was noted that the the level of GFP fluorescence from lysosomal-dPIP4K::eGFP was observed to be very low in the salivary glands and did not interfere with our analysis PIP_3 measurements using the GFP::PH-GRP1 probe in Figure 3D. Using GIBSON assembly, we added a C-terminal CAAX motif to the PIP4K2B fragment amplified from PIP4K2B::eGFP (kind gift from Jonathan Clarke, Uni. Of Cambridge) and cloned the fusion construct into pEGFP-C1 vector

between *NheI* and BamHI sites to generate PIP4K2B::mCherryCAAX. The localization of PIP4K2B::eGFP and PIP4K2B::mCherryCAAX was confirmed using confocal microscopy as described before. All primer sequences used for cloning are available on request.

mRNA quantification using qPCR analysis—RNA from 3 wandering third instar larvae was extracted using standard TRIzol – chloroform method. cDNA was synthesized from 1 μg of RNA using Superscript II reverse transcriptase (Invitrogen). A no reverse transcription control sample was also included for each genotype. qPCR analysis was performed on an Applied Biosystems 7500 fast qPCR system using diluted cDNA samples and primers against genes of interest and *rp49* as internal controls. The C_t values obtained for different genes were normalized to those of *rp49* from the same sample.

Cell Culture, RNAi and Insulin stimulation—CHO cell line stably expressing insulin receptor (isoform A) was a kind gift from Dr Nicholas Webster, UCSD. These were maintained at standard conditions in HF12 culture medium supplemented with 10% Foetal bovine serum and under G418 selection (400 μg/ml). Transfections were done 48 hr. before the assay using FuGene as per manufacturer's protocols when the cultures were 50% confluent. For insulin stimulation assays, cells were starved overnight in HF12 medium without serum. Thereafter, the cells were de-adhered, collected into eppendorf tubes and stimulated with 1 μM insulin for indicated times. Post stimulation, cells were spun down and lysed immediately.

S2R+ cells were cultured in Schneider's medium supplemented with 10% non-heat inactivated fetal bovine serum and contained antibiotics – streptomycin and penicillin. dsRNA was synthesized in-house using Megascript RNAi Kit as per manufacturer's instructions. For dsRNA treatments, 0.5 X 10^6 cells were seeded into a 24-well plate. Once observed to be settled, cells were incubated with incomplete medium containing 1.875 μg of dsRNA. After 1 hour, an equal amount of complete medium was added to each well. The same procedure was repeated on each well 48 hours after initial transfection after removal of the spent medium from each well. Cells were harvested by trypsinization after a total of 96 hours of dsRNA treatment. For mass spectrometric estimation of PIP_3, S2R+ cells were pelleted down and stimulated with 1 μM insulin for 10 min after a short 20 min starvation. The reaction was stopped by the addition of ice-cold initial organic mix (described later in the section) and used for lipid extraction.

Larval growth curve analysis—Adult flies were made to lay eggs within a span of 4-6 hr on normal food. The protocol followed for transfer of larvae onto vials containing different diets is described in Figures S6A and S6D. For experiment indicated in Figure S6B, vials had around 15-25 larvae. For the experiment depicted in Figures 5H–5K, the vials had about 7-10 larvae. The values for pupariation were plotted after normalizing to the maximum percentage of pupariation achieved in each vial. For data in Figure S6B, mean pupariation percentage was calculated for each time bin and plotted with SD as errors. For Figures 5H–5K, every measurement was plotted and thereafter fitted to a variable slope on Graph Pad Prism (ver. 5)

Hemolymph Trehalose Measurements—The measurements were done as first described in Musselman et al. (2011). Hemolymph was pooled from five to eight larvae to obtain 1 μL for assay. 1 μl hemolymph was diluted in 25 μl 0.25 M Sodium Bicarbonate and heated at 95°C for 2 hr, brought down to room temperature. Further, 66 μl of 0.25 M sodium acetate and 8 μl 1M acetic acid was added to the 25 μl from the previous step to form the digestion mix. 40 μl of this mix was digested with 1 μl of Porcine Trehalase at 37°C overnight. The concentration of digested trehalose was measured from 10 μl of digested sample against glucose standards using the glucose (GO) assay kit.

Cell size analysis in salivary glands—Salivary glands were dissected from wandering third instar larvae and fixed in 4% paraformaldehyde for 30 min at 4°C. Post fixation, glands were washed thrice with 1X PBS and incubated in BODIPY-FL-488 for 3 hours at room temperature. The glands were washed thrice in 1X PBS following which nuclei were labeled (using either DAPI or TOTO3) for 10 mins at room temperature and washed with 1X PBS again. The glands were then mounted in 70% glycerol and imaged within a day of mounting. Imaging was done on Olympus FV1000 Confocal LSM using a 20x objective. The images were then stitched into a 3D projection using an ImageJ plugin. These reconstituted 3D z stacks were then analyzed for nuclei numbers (correlate for cell number) and volume of the whole gland using Volocity Software (version 5.5.1, Perkin Elmer Inc.). The average cell size was calculated as the ratio of the average volume of the gland to the number of nuclei.

Imaging PIP_3 probe in larval tissues—For experiments with salivary glands, wandering third instar larvae were dissected one larva at a time and glands were immediately dropped into one well of a 96-well plate containing either only PBS or PBS + 10 μM Insulin (75 μl) and incubated for 10 min at room temperature. Following this, 25 μl of 16% PFA was added into the same well to yield a final conc. of 4% PFA. The glands were fixed in this solution for 15 min at room temperature and then transferred sequentially to wells containing PBS every 10 min for 3 washes. Finally, glands were mounted in 80% glycerol in PBS containing antifade (0.4% propyl-gallate). For experiments with fat body lobes, late third instar feeding larvae were starved by placing them on a filter paper soaked in 1X PBS for 2 hr. Thereafter, the incubation, fixation and mounting steps were done exactly as described for salivary glands. Imaging was done on LSM 780 inverted confocal microscope with a 20X/0.8 NA Plan Apochromat objective.

For live imaging, salivary glands from wandering third instar larvae were dissected (glands from one larva imaged in one imaging run) and placed inside a drop of imaging buffer (1X PBS containing 2mg/ml glucose) on a coverglass. The buffer was slowly and carefully soaked out with a paper tissue to let the glands settle and adhere to the surface. Thereafter, the glands were immediately rehydrated with 25 μl of imaging buffer. The imaging was done on Olympus FV3000 LSM confocal system using a 10X objective. A total of 80 frames of a single plane were acquired at 10 s intervals. While imaging, 25 μl of 20uM (2X) bovine insulin was used to stimulate the glands. After the steady state was achieved, 50 μl of 800nM (2X) of wortmannin was added on top to inhibit PI3K activity.

Immunostaining of larval brains—Brains were dissected out from wandering third instar larvae in 1X PBS and fixed in 4% Paraformaldehyde for 30 min at room temperature,

permeabilised with 0.3% Triton X-100 solution in PBS (0.3% PBTx) and incubated overnight with dILP2 antibody at 1:200 dilution. Following day, the brains were washed thrice in 0.3% PBTx and incubated with Alexa fluor-conjugated secondary antibody (Thermo Scientific Inc., 1:200 dilution) for 4 hr at room temperature. Following this, DAPI staining was done for 10 min. The brains were again washed extensively in 0.3% PBTx, mounted in 70% Glycerol and imaged on the Zeiss LSM 780 confocal microscope using the 20X objective.

LCMS based PIP_2 and PIP_3 measurements—To test if the probe-based imaging of PIP_3 in single cells indeed reflects *in vivo* changes across the animal, we refined and adapted existing protocols (Clark et al., 2011) to perform mass spectrometric measurements of PIP_3 from *Drosophila* S2R+ cells and whole larval lipid extracts (Scheme depicted in Figure S1E). The amount of PIP_3 that has been detected and quantified from biological samples is in the range of a few tens of picomoles (Malek et al., 2017). We coupled liquid chromatography to high sensitivity mass spectrometry (LCMS) and used a Multiple Reaction Monitoring (MRM) method to detect PIP_3 standards for reliable quantification down to a few femtomoles (ca. 10 fmol, the lowest point in the figure inset on the standard curve in Figure S1D. Since cellular lipids are composed of molecular species with varying acyl chain lengths, we first characterized the PIP_3 species from *Drosophila* whole larval extracts through use of neutral loss scans and thereafter quantified the abundance of these species. Figure S1F depicts the elution profiles of the different PIP_3 species from *Drosophila* larvae that were reproducibly detected across samples and Figure S2Ai shows the relative abundance of various PIP_3 species. The 34:2 PIP_3 species was found to be the most abundant. To standardize the procedure, we bisected whole larvae, stimulated them with insulin and measured the levels of various PIP_3 species between samples with and without insulin stimulation. Our LCMS method could clearly detect an increase in the levels of all the identified PIP_3 species upon insulin stimulation (Figure S2Aii). Similar process was followed for identification and characterization of PIP_3 species from S2R+ cells and the identification of PIP_2 from both S2R+ cells and larval samples. A detailed description of the steps involved in the whole procedure is given below:

Lipid extraction—5 larvae were dissected in 1X PBS (or cells pelleted from a single well) and transferred immediately into 37.5 µl of 1X PBS in a 2 mL Eppendorf. For insulin stimulation, to this, 37.5 µl of 100 µM Insulin for larval samples (final concentration – 50 µM) and 2 µM Insulin for cells (final concentration – 1 µM) was added and the tube was incubated on a mix mate shaker for 10 min at 500 rpm. At the end of incubation time, 750 µl of ice-cold 2:1 MeOH:$CHCl_3$ organic mix was added to stop the reaction. In the case of larval samples, part of this solution was decanted and the rest of the mix containing larval tissues was transferred into a homogenization tube. Larval tissues were homogenized in 4 cycles of 10 s with 30 s intervals at 6000 rpm in a homogenizer (Precellys, Bertin Technologies). The tubes were kept on ice at all intervals (No homogenization was required for cell culture samples). The entire homogenate was then transferred to a fresh eppendorf and the homogenization tube was then washed with the decanted mix kept aside earlier. 120 µl of water was added to the homogenate collected in eppendorf, followed by the addition of 5 ng of 17:0, 20:4 PIP_3 internal standard (ISD). The mixture was vortexed and 725 µl of

chloroform was added to it. After vortexing again for 2 min at around 1000-1500 rpm, the phases were separated by centrifugation for 3 min at 1500 g. 1ml (1.2 mL for cells) of the lower organic phase was removed and stored in a fresh tube. In the case of larval samples, to the remaining aqueous upper phase, 725 µl of chloroform was again added. The mixture was vortexed and spun down to separate the phases. Again, 1 mL of the organic phase was collected and pooled with the previous collection (total of 2ml). (For cell culture samples, only one round of neutral lipid extraction is sufficient). This organic phase was used for measuring total organic phosphate. To the aqueous phase, 500 µl of the initial organic mix was added followed by 170 µl of 2.4M HCl and 500 µl of $CHCl_3$. This mixture was vortexed for 5 min at 1000-1500 rpm and allowed to stand at room temperature for 5 minutes. The phases were separated by centrifugation (1500 g, 3 min). The lower organic phase was collected into a fresh tube by piercing through the protein band sitting at the interface. To this, 708 µl of lower phase wash solution was added, the mixture was vortexed and spun down (1500 g, 3 min). The resultant lower organic phase was completely taken out carefully into an Eppendorf tube and used for derivatization reaction.

Extraction solvent mixtures—Initial organic mix: MeOH/Chloroform in the ratio of 484/242 ml, Lower Phase Wash Solution: Methanol/1 M hydrochloric acid/ chloroform in a ratio of 235/245/15 ml. All ratios are expressed as vol/vol/vol.

Derivatization of Lipids—To the organic phase of the sample, 50 µl of 2M TMS-Diazomethane was added (TO BE USED WITH ALL SAFETY PRECAUTIONS!). The reaction was allowed to proceed at room temperature for 10 min at 600 rpm. After 10 min, 10 µl of Glacial acetic acid was added to quench the reaction, vortexed briefly and spun down. 700 µl of post derivatization wash solvent was then added to the sample, vortexed (2 min, 1000-1500 rpm) and spun down. The upper aqueous phase was discarded and the wash step was repeated. To the final organic phase, 100 µl of 9:1 MeOH:H_2O mix was added and the sample was dried down to about 10-15 µl in a speedvac under vacuum.

Chromatography and Mass spectrometry—The larval lipid extracts were re-suspended in 170 µl LC-MS grade methanol and 30 µl LC-MS grade water (80 µl methanol and 20 ul water for cell culture samples). Samples were injected as duplicate runs of 3.5 (stimulated) or 7 µl (unstimulated) for PIP_3 measurements and 2 ul injections for PIP_2 measurements. Chromatographic separation was performed on an Acquity UPLC BEH300 C4 column (100 × 1.0 mm; 1.7 µm particle size) purchased from Waters Corporation, USA on a Waters Aquity UPLC system and detected using an ABSCIEX 6500 QTRAP mass spectrometer. The flow rate was 100 µL/min. Gradients were run starting from 55% Buffer A (Water + 0.1% Formic Acid)- 45% Buffer B (Acetonitrile + 0.1% Formic acid) from 0-5 min; thereafter 45% B to 100% B from 5-10 min; 100% B was held from 10-15 min; brought down from 100% B to 45% B between 15-16 min and held there till 20th min to re-equilibrate the column. On the mass spectrometer, in pilot standardization experiments, we first employed Neutral Loss Scans on biological samples to look for parent ions that would lose neutral fragments of 598 a.m.u indicative of PIP_3 lipid species and 490 a.m.u indicative of PIP_2 species (as described in (Clark et al., 2011)). Thereafter, these PIP_2 and PIP_3 species were quantified in biological samples using the selective Multiple Reaction Monitoring

(MRM) method in the positive mode. For PIP_3, only those MRM transitions that showed an increase upon insulin stimulation of biological samples were used for the final experiments (depicted in Figure S2Aii). Area of all the peaks was calculated on Sciex MultiQuant software. The area of the internal standard peak was used to normalize for lipid recovery during extraction. The normalized area for each of the species was then divided by the amount of organic phosphate measured in each of the biological samples. The other mass spectrometer parameters are as follows:

For PIP_3, ESI voltage: +5100 V; Dwell time: 60-65 ms; DP (De-clustering Potential): 35.0 V; EP: (Entrance Potential): 10.1 V, CE (Collision Energy): 47.0-50.0 V; CXP (Collision cell Exit Potential): 11.6-12.0 V, Source Temperature: 350 C, Curtain Gas: 35.0, GS1: 15, GS2: 15.

For PIP_2, ESI voltage: +5100-5200 V; Dwell time: 35-65 ms; DP (De-clustering Potential): 60.0 V; EP: (Entrance Potential): 11.0 V, CE (Collision Energy): 37.0 V; CXP (Collision cell Exit Potential): 15.0 V, Source Temperature: 300 C, Curtain Gas: 35-37.0, GS1:15-20, GS2: 15-20.

The MRM mass pairs used for PIP_2 and PIP_3 species identification and quantification are listed below:

Europe PMC Funders Author Manuscripts

	Sample							
	Drosophila Larvae				S2R+ cells			
	Acyl species	PIP_3 Parent Ion	PIP_2 Parent Ion	Daughter Ion	Acyl species	PIP_3 Parent Ion	PIP_2 Parent Ion	Daughter Ion
MRM Transitions	32_1	1147.5	1039.5	549.5	30_1	1119.5	1011.5	521.5
	32_2	1145.5	1037.5	547.5	30_3	-	1007.5	517.5
	34_1	1175.5	1067.5	577.5	30_4	-	1005.5	515.5
	34_2	1173.5	1065.5	575.5	32_0	1149.5	1041.5	551.5
	34_3	1171.5	1063.5	573.5	32_1	1147.5	1039.5	549.5
	36_1	1203.5	1095.5	605.5	32_2	1145.5	1037.5	547.5
	36_2	1201.5	1093.5	603.5	32_3	-	1035.5	545.5
	36_3	1199.5	1091.5	601.5	34_0	1177.5	1069.5	579.5
	36_4	1197.5	1089.5	599.5	34_1	1175.5	1067.5	577.5
					34_2	1173.5	1065.5	575.5
					34_3	1171.5	1063.5	573.5
					34_4	1169.5	1061.5	571.5
					34_5	1167.5	1059.5	569.5
					36_0	-	1097.5	607.5
					36_1	-	1095.5	605.5
					36_2	1201.5	1093.5	603.5
					36_3	1199.5	1091.5	601.5
					36_4	1197.5	1089.5	599.5
					36_5	1195.5	1087.5	597.5

Europe PMC Funders Author Manuscripts

Sample							
Drosophila Larvae				S2R+ cells			
Acyl species	PIP_3 Parent Ion	PIP_2 Parent Ion	Daughter Ion	Acyl species	PIP_3 Parent Ion	PIP_2 Parent Ion	Daughter Ion
				38_0	-	1125.5	635.5
				38_2	-	1121.5	631.5
				38_3	1227.5	1119.5	629.5
				38_4	1225.5	1117.5	627.5
				38_5	1223.5	1115.5	625.5
				37_4 ISD	1211.5	-	613.5

Total Organic Phosphate measurement—800 μl (larval samples) or 1 mL (cell samples) of the organic phase from each sample was taken into phosphate-free glass tubes and dried completely at 90°C. Tubes containing phosphate standard (KH_2PO_4 – 7.34 mM stock) in the range of 3.67 nmol to 198.18 nmol were also dried at 120°C. After the addition of 50 μl of 70% perchloric acid was to all the tubes containing the standards and samples, the tubes were heated at 180°C for 30 min and thereafter cooled to room temperature. This

was followed by the addition of 250 μl water, 50 μl of 2.5% Ammonium molybdate and 50 μl of 10% Ascorbic acid into each tube and incubation at 37°C for 1 h. The absorbance of the solution in each tube was measured using 130 μl of each sample at 630 nm.

***In vitro* PI5P4-kinase assay with cell lysates—**The S2R+ cells were pelleted at 1000 g for 10 min and washed with ice-cold PBS Twice. Thereafter, cells were homogenized in lysis buffer containing 50mM Tris-Cl, pH – 7.5, 1mM EDTA, 1mM EGTA, 1% Triton X-100, 50mM NaF, 0.27 M Sucrose, 0.1% β-Mercaptoethanol with freshly added protease and phosphatase inhibitors (Roche). The lysate was then centrifuged at 1000 g for 15 min at 4°C. Protein estimation was performed using the Bradford reagent according to the manufacturer's instructions.

Vacuum-dried substrate lipid (6 μM PI5P) and 20 μM of phosphatidylserine were resuspended in 10 mM Tris pH 7.4 and micelles were formed by sonication for 2 min in a bath-sonicator. 50 μl of 2 x PIP-kinase reaction buffer (100 mM Tris pH 7.4, 20 mM $MgCl_2$, 140 mM KCl, and 2 mM EGTA) containing 20 μM ATP, 5 μCi [γ-^{32}P] ATP and cell lysates containing ~10 μg total protein was added to the micelles. The reaction mixture was incubated at 30°C for 16 h. Lipids were extracted and resolved by one-dimensional TLC (45:35:8:2 chloroform: methanol: water: 25% ammonia). The resolved lipids were imaged using phosphorImager.

Western Blotting—For larval western blots, lysates were prepared by homogenizing 3 wandering third instar larvae or 5 pairs of salivary glands from wandering third instar larvae. In the case of CHO-IR and S2R+ cells, pelleted cells were lysed by repeated pipetting in lysis buffer (same as described above). Thereafter, the samples were heated at 95°C with Laemli loading buffer for 5 min and loaded onto an SDS- Polyacrylamide gel. The proteins were subsequently transferred onto a nitrocellulose membrane and incubated with indicated antibodies overnight at 4°C (for actin/tubulin incubation was done at room temperature for 3 hr.). For stripping and re-probing, blots were incubated in a total of 30 mL 3% Glacial acetic acid over 1 hr (10 mL X 3 times, 20 min each), washed extensively [1 hr, 4 X10ml of Tris Buffer Saline containing 0.1% Tween-20 (0.1% TBST)], incubated in blocking solution again for 15 min and thereafter re-probed with next primary antibody. Primary antibody concentrations used were – anti - α-actin, 1:1000; anti- dPIP4K, 1:1000; anti – GAPDH, 1:1000; anti - PIP4KB, 1:1000; anti – pAKT^{T308}, 1:1000; anti-AKT, 1:1000; anti-pAKT^{T342}, 1:1000; anti-pS6K^{T398}, 1:1000. The blots were then washed thrice with 0.1% TBS-T and incubated with 1:10000 concentration of appropriate HRP-conjugated secondary antibodies (Jackson Laboratories, Inc.) for 1.5 hr. After three washes with 0.1% TBS-T, blots were developed using Clarity Western ECL substrate (Biorad) on a GE ImageQuant LAS 4000 system.

Quantification and Statistical Analysis

PIP_3 quantification from imaging experiments—Confocal slices were manually curated to generate maximum z-projections of middle few planes of cells. Thereafter, line profiles were drawn across clearly identifiable plasma membrane regions and their adjacent cytosolic regions and ratios of mean intensities for these line profiles were calculated for

each cell. For salivary glands, about cells from multiple glands were analyzed and used to generate statistics. For fat body, about cells inmany regions from multiple animals were used for analysis.

PIP_3 quantification from mass spectrometry measurements—The area under the peaks for individual lipid species was extracted using MultiQuant software. Numerical analysis was done in Microsoft Excel. The area was normalized to the value of organic phosphate recovered from the sample.

Densitometry analysis of western blots—Analysis was performed using the ImageJ software. First, the background intensities were subtracted from the images using an average of mean background intensities of a few ROIs adjacent to band of interest. Thereafter, ROIs were drawn around the bands of interest and the integrated intensity of each ROI was extracted from the image. The loading control bands were analyzed in the same manner. Further numerical analyses to obtain ratios of different band intensities were performed in Microsoft Excel.

Sampling and Statistical analysis—Each experiment was performed unblinded on different biological groups with multiple biological replicates. No statistical analysis was done *a priori* to determine the sample sizes. For most comparisons, with the range of sample sizes the experiments could be performed with at a given time, it was not possible to be sure of the normality of distribution. Hence, the non-parametric *Mann-Whitney Test* was used to compare the differences in medians of sample populations. For mass spectrometric lipid measurements from larvae done using three biological replicates per genotype, *Student's t test* was used to check for differences in means between samples of different genotypes (Figures 1C and 1F). One-way ANOVA with post hoc Tukey's pairwise comparison was used whenever the experiment consisted of more than two biological groups.

Supplementary Material

Refer to Web version on PubMed Central for supplementary material.

Acknowledgments

This work was supported by the National Centre for Biological Sciences, TIFR (India), Department of Biotechnology, Ministry of Science and Technology (India) (BT/PR6354/BRB/10/1127/2012), and a Wellcome Trust-DBT India Alliance Senior Fellowship (IA/S/14/2/501540 to P.R.). S.S. is a recipient of the CSIR S.P. Mukherji Fellowship (SPM-07/860(0118)/2012-EMR-I) and S.M. an ICMR Fellowship (45/08/2014/CMB/BMS). We also thank Avishek Ghosh, Chaitra Prabhakara, Thomas Van Zanten, and Parijat Sil for extensive discussions on the manuscript and experiments. We also thank Revathi Ramdas and Sreedevi Raghu for assistance with experiments. We also thank the NCBS *Drosophila*, Imaging (CIFF), and Lipidomics Facilities for support.

References

Alessi DR, James SR, Downes CP, Holmes AB, Gaffney PR, Reese CB, Cohen P. Characterization of a 3-phosphoinositide-dependent protein kinase which phosphorylates and activates protein kinase Balpha. Curr Biol. 1997; 7:261–269. [PubMed: 9094314]

Auger KR, Serunian LA, Soltoff SP, Libby P, Cantley LC. PDGF-dependent tyrosine phosphorylation stimulates production of novel polyphosphoinositides in intact cells. Cell. 1989; 57:167–175. [PubMed: 2467744]

Balakrishnan SS, Basu U, Raghu P. Phosphoinositide signalling in Drosophila. Biochim Biophys Acta. 2015; 1851:770–784. [PubMed: 25449646]

Barbieri M, Bonafè M, Franceschi C, Paolisso G. Insulin/IGF-I-signaling pathway: an evolutionarily conserved mechanism of longevity from yeast to humans. Am J Physiol Endocrinol Metab. 2003; 285:E1064–E1071. [PubMed: 14534077]

Böhni R, Riesgo-Escovar J, Oldham S, Brogiolo W, Stocker H, Andruss BF, Beckingham K, Hafen E. Autonomous control of cell and organ size by CHICO, a Drosophila homolog of vertebrate IRS1-4. Cell. 1999; 97:865–875. [PubMed: 10399915]

Britton JS, Lockwood WK, Li L, Cohen SM, Edgar BA. Drosophila's insulin/PI3-kinase pathway coordinates cellular metabolism with nutritional conditions. Dev Cell. 2002; 2:239–249. [PubMed: 11832249]

Brogiolo W, Stocker H, Ikeya T, Rintelen F, Fernandez R, Hafen E. An evolutionarily conserved function of the Drosophila insulin receptor and insulin-like peptides in growth control. Curr Biol. 2001; 11:213–221. [PubMed: 11250149]

Bulley SJ, Droubi A, Clarke JH, Anderson KE, Stephens LR, Hawkins PT, Irvine RF. In B cells, phosphatidylinositol 5-phosphate 4-kinase-α synthesizes PI(4,5)P2 to impact mTORC2 and Akt signaling. Proc Natl Acad Sci USA. 2016; 113:10571–10576. [PubMed: 27601656]

Carricaburu V, Lamia KA, Lo E, Favereaux L, Payrastre B, Cantley LC, Rameh LE. The phosphatidylinositol (PI)-5-phosphate 4-kinase type II enzyme controls insulin signaling by regulating PI-3,4,5-trisphosphate degradation. Proc Natl Acad Sci USA. 2003; 100:9867–9872. [PubMed: 12897244]

Church RB, Robertson FW. Biochemical analysis of genetic differences in the growth of Drosophila. Genet Res. 1966; 7:383–407. [PubMed: 5940873]

Clark J, Anderson KE, Juvin V, Smith TS, Karpe F, Wakelam MJO, Stephens LR, Hawkins PT. Quantification of PtdInsP3 molecular species in cells and tissues by mass spectrometry. Nat Methods. 2011; 8:267–272. [PubMed: 21278744]

Clarke JH, Wang M, Irvine RF. Localization, regulation and function of type II phosphatidylinositol 5-phosphate 4-kinases. Adv Enzyme Regul. 2010; 50:12–18. [PubMed: 19896968]

Clément S, Krause U, Desmedt F, Tanti JF, Behrends J, Pesesse X, Sasaki T, Penninger J, Doherty M, Malaisse W, et al. The lipid phosphatase SHIP2 controls insulin sensitivity. Nature. 2001; 409:92–97. [PubMed: 11343120]

Colombani J, Raisin S, Pantalacci S, Radimerski T, Montagne J, Léopold P. A nutrient sensor mechanism controls Drosophila growth. Cell. 2003; 114:739–749. [PubMed: 14505573]

Durán RV, Hall MN. Regulation of TOR by small GTPases. EMBO Rep. 2012; 13:121–128. [PubMed: 22240970]

Elong Edimo W, Schurmans S, Roger PP, Erneux C. SHIP2 signaling in normal and pathological situations: Its impact on cell proliferation. Adv Biol Regul. 2014; 54:142–151. [PubMed: 24091101]

Emerling BM, Hurov JB, Poulogiannis G, Tsukazawa KS, Choo-Wing R, Wulf GM, Bell EL, Shim HS, Lamia KA, Rameh LE, et al. Depletion of a putatively druggable class of phosphatidylinositol kinases inhibits growth of p53-null tumors. Cell. 2013; 155:844–857. [PubMed: 24209622]

Fruman DA, Chiu H, Hopkins BD, Bagrodia S, Cantley LC, Abraham RT. The PI3K pathway in human disease. Cell. 2017; 170:605–635. [PubMed: 28802037]

Géminard C, Rulifson EJ, Léopold P. Remote control of insulin secretion by fat cells in Drosophila. Cell Metab. 2009; 10:199–207. [PubMed: 19723496]

Georgiev P, Okkenhaug H, Drews A, Wright D, Lambert S, Flick M, Carta V, Martel C, Oberwinkler J, Raghu P. TRPM channels mediate zinc homeostasis and cellular growth during Drosophila larval development. Cell Metab. 2010; 12:386–397. [PubMed: 20889130]

Grainger DL, Tavelis C, Ryan AJ, Hinchliffe KA. Involvement of phosphatidylinositol 5-phosphate in insulin-stimulated glucose uptake in the L6 myotube model of skeletal muscle. Pflugers Arch. 2011; 462:723–732. [PubMed: 21847559]

Gual P, Le Marchand-Brustel Y, Tanti J-F. Positive and negative regulation of insulin signaling through IRS-1 phosphorylation. Biochimie. 2005; 87:99–109. [PubMed: 15733744]

Gupta A, Toscano S, Trivedi D, Jones DR, Mathre S, Clarke JH, Divecha N, Raghu P. Phosphatidylinositol 5-phosphate 4-kinase (PIP4K) regulates TOR signaling and cell growth during Drosophila development. Proc Natl Acad Sci USA. 2013; 110:5963–5968. [PubMed: 23530222]

Haruta T, Uno T, Kawahara J, Takano A, Egawa K, Sharma PM, Olefsky JM, Kobayashi M. A rapamycin-sensitive pathway down-regulates insulin signaling via phosphorylation and proteasomal degradation of insulin receptor substrate-1. Mol Endocrinol. 2000; 14:783–794. [PubMed: 10847581]

Hawkins PT, Stephens LR. PI3K signalling in inflammation. Biochim Biophys Acta. 2015; 1851:882–897. [PubMed: 25514767]

Hawkins PT, Anderson KE, Davidson K, Stephens LR. Signalling through Class I PI3Ks in mammalian cells. Biochem Soc Trans. 2006; 34:647–662. [PubMed: 17052169]

Jones DR, Foulger R, Keune W-J, Bultsma Y, Divecha N. PtdIns5P is an oxidative stress-induced second messenger that regulates PKB activation. FASEB J. 2013; 27:1644–1656. [PubMed: 23241309]

Kamalesh K, Trivedi D, Toscano S, Sharma S, Kolay S, Raghu P. Phosphatidylinositol 5-phosphate 4-kinase regulates early endosomal dynamics during clathrin-mediated endocytosis. J Cell Sci. 2017; 130:2119–2133. [PubMed: 28507272]

Kelly KL, Ruderman NB. Insulin-stimulated phosphatidylinositol 3-kinase. Association with a 185-kDa tyrosine-phosphorylated protein (IRS-1) and localization in a low density membrane vesicle. J Biol Chem. 1993; 268:4391–4398. [PubMed: 8382701]

Kolay S, Basu U, Raghu P. Control of diverse subcellular processes by a single multi-functional lipid phosphatidylinositol 4,5-bisphosphate [PI(4,5)P2]. Biochem J. 2016; 473:1681–1692. [PubMed: 27288030]

Lamia KA, Peroni OD, Kim YB, Rameh LE, Kahn BB, Cantley LC. Increased insulin sensitivity and reduced adiposity in phosphatidylinositol 5-phosphate 4-kinase beta-/- mice. Mol Cell Biol. 2004; 24:5080–5087. [PubMed: 15143198]

Lizcano JM, Alrubaie S, Kieloch A, Deak M, Leevers SJ, Alessi DR. Insulin-induced Drosophila S6 kinase activation requires phosphoinositide 3-kinase and protein kinase B. Biochem J. 2003; 374:297–306. [PubMed: 12841848]

Luo J, Cantley LC. The negative regulation of phosphoinositide 3-kinase signaling by p85 and it's implication in cancer. Cell Cycle. 2005; 4:1309–1312. [PubMed: 16131837]

Mackey AM, Sarkes DA, Bettencourt I, Asara JM, Rameh LE. PIP4kγ is a substrate for mTORC1 that maintains basal mTORC1 signaling during starvation. Sci Signal. 2014; 7:ra104. [PubMed: 25372051]

Madsen RR, Vanhaesebroeck B, Semple RK. Cancer-Associated PIK3CA Mutations in Overgrowth Disorders. Trends Mol Med. 2018; 24:856–870. [PubMed: 30197175]

Malek M, Kielkowska A, Chessa T, Anderson KE, Barneda D, Pir P, Nakanishi H, Eguchi S, Koizumi A, Sasaki J, et al. PTEN Regulates PI(3,4)P_2 Signaling Downstream of Class I PI3K. Mol Cell. 2017; 68:566–580.e10. [PubMed: 29056325]

Mathre S, Reddy KB, Ramya V, Krishnan H, Ghosh A, Raghu P. Functional analysis of the biochemical activity of mammalian phosphatidylinositol 5 phosphate 4-kinase enzymes. Biosci Rep. 2019; 39

Menon S, Dibble CC, Talbott G, Hoxhaj G, Valvezan AJ, Takahashi H, Cantley LC, Manning BD. Spatial control of the TSC complex integrates insulin and nutrient regulation of mTORC1 at the lysosome. Cell. 2014; 156:771–785. [PubMed: 24529379]

Musselman LP, Fink JL, Narzinski K, Ramachandran PV, Hathiramani SS, Cagan RL, Baranski TJ. A high-sugar diet produces obesity and insulin resistance in wild-type Drosophila. Dis Model Mech. 2011; 4:842–849. [PubMed: 21719444]

Nässel DR, Vanden Broeck J. Insulin/IGF signaling in Drosophila and other insects: factors that regulate production, release and post-release action of the insulin-like peptides. Cell Mol Life Sci. 2016; 73:271–290. [PubMed: 26472340]

O'Reilly KE, Rojo F, She QB, Solit D, Mills GB, Smith D, Lane H, Hofmann F, Hicklin DJ, Ludwig DL, et al. mTOR inhibition induces upstream receptor tyrosine kinase signaling and activates Akt. Cancer Res. 2006; 66:1500–1508. [PubMed: 16452206]

Pagliarini DJ, Worby CA, Dixon JE. A PTEN-like phosphatase with a novel substrate specificity. J Biol Chem. 2004; 279:38590–38596. [PubMed: 15247229]

Paradis S, Ailion M, Toke A, Thomas JH, Ruvkun G. A PDK1 homolog is necessary and sufficient to transduce AGE-1 PI3 kinase signals that regulate diapause in Caenorhabditis elegans. Genes Dev. 1999; 13:1438–1452. [PubMed: 10364160]

Pasco MY, Léopold P. High sugar-induced insulin resistance in Drosophila relies on the lipocalin Neural Lazarillo. PLoS ONE. 2012; 7:e36583. [PubMed: 22567167]

Rameh LE, Tolias KF, Duckworth BC, Cantley LC. A new pathway for synthesis of phosphatidylinositol-4,5-bisphosphate. Nature. 1997; 390:192–196. [PubMed: 9367159]

Rintelen F, Stocker H, Thomas G, Hafen E. PDK1 regulates growth through Akt and S6K in Drosophila. Proc Natl Acad Sci USA. 2001; 98:15020–15025. [PubMed: 11752451]

Sarkes D, Rameh LE. A novel HPLC-based approach makes possible the spatial characterization of cellular PtdIns5P and other phosphoinositides. Biochem J. 2010; 428:375–384. [PubMed: 20370717]

Sato M, Ueda Y, Umezawa Y. Imaging diacylglycerol dynamics at organelle membranes. Nat Methods. 2006; 3:797–799. [PubMed: 16990811]

Shim H, Wu C, Ramsamooj S, Bosch KN, Chen Z, Emerling BM, Yun J, Liu H, Choo-Wing R, Yang Z, et al. Deletion of the gene Pip4k2c, a novel phosphatidylinositol kinase, results in hyperactivation of the immune system. Proc Natl Acad Sci USA. 2016; 113:7596–7601. [PubMed: 27313209]

Shingleton AW, Das J, Vinicius L, Stern DL. The temporal requirements for insulin signaling during development in Drosophila. PLoS Biol. 2005; 3:e289. [PubMed: 16086608]

Song MS, Salmena L, Pandolfi PP. The functions and regulation of the PTEN tumour suppressor. Nat Rev Mol Cell Biol. 2012; 13:283–296. [PubMed: 22473468]

Stephens LR, Hughes KT, Irvine RF. Pathway of phosphatidylinositol(3,4,5)-trisphosphate synthesis in activated neutrophils. Nature. 1991; 351:33–39. [PubMed: 1851250]

Tremblay F, Brûlé S, Hee Um S, Li Y, Masuda K, Roden M, Sun XJ, Krebs M, Polakiewicz RD, Thomas G, Marette A. Identification of IRS-1 Ser-1101 as a target of S6K1 in nutrient- and obesity-induced insulin resistance. Proc Natl Acad Sci USA. 2007; 104:14056–14061. [PubMed: 17709744]

Um SH, Frigerio F, Watanabe M, Picard F, Joaquin M, Sticker M, Fumagalli S, Allegrini PR, Kozma SC, Auwerx J, Thomas G. Absence of S6K1 protects against age- and diet-induced obesity while enhancing insulin sensitivity. Nature. 2004; 431:200–205. [PubMed: 15306821]

Vanhaesebroeck B, Stephens L, Hawkins P. PI3K signalling: the path to discovery and understanding. Nat Rev Mol Cell Biol. 2012; 13:195–203. [PubMed: 22358332]

Wang DG, Paddock MN, Lundquist MR, Sun JY, Mashadova O, Amadiume S, Bumpus TW, Hodakoski C, Hopkins BD, Fine M, et al. PIP4Ks Suppress Insulin Signaling through a Catalytic-Independent Mechanism. Cell Rep. 2019; 27:1991–2001. [PubMed: 31091439]

Wullschleger S, Loewith R, Hall MN. TOR signaling in growth and metabolism. Cell. 2006; 124:471–484. [PubMed: 16469695]

Europe PMC Funders Author Manuscripts

Highlights

- *Drosophila* PIP4K mutant larvae have increased PIP_3 levels in cells
- Cells show enhanced sensitivity to insulin in the absence of PIP4K
- PIP4K regulates enzymes involved in PIP_3 turnover at the plasma membrane
- Loss of PIP4K suppresses insulin resistance phenotypes

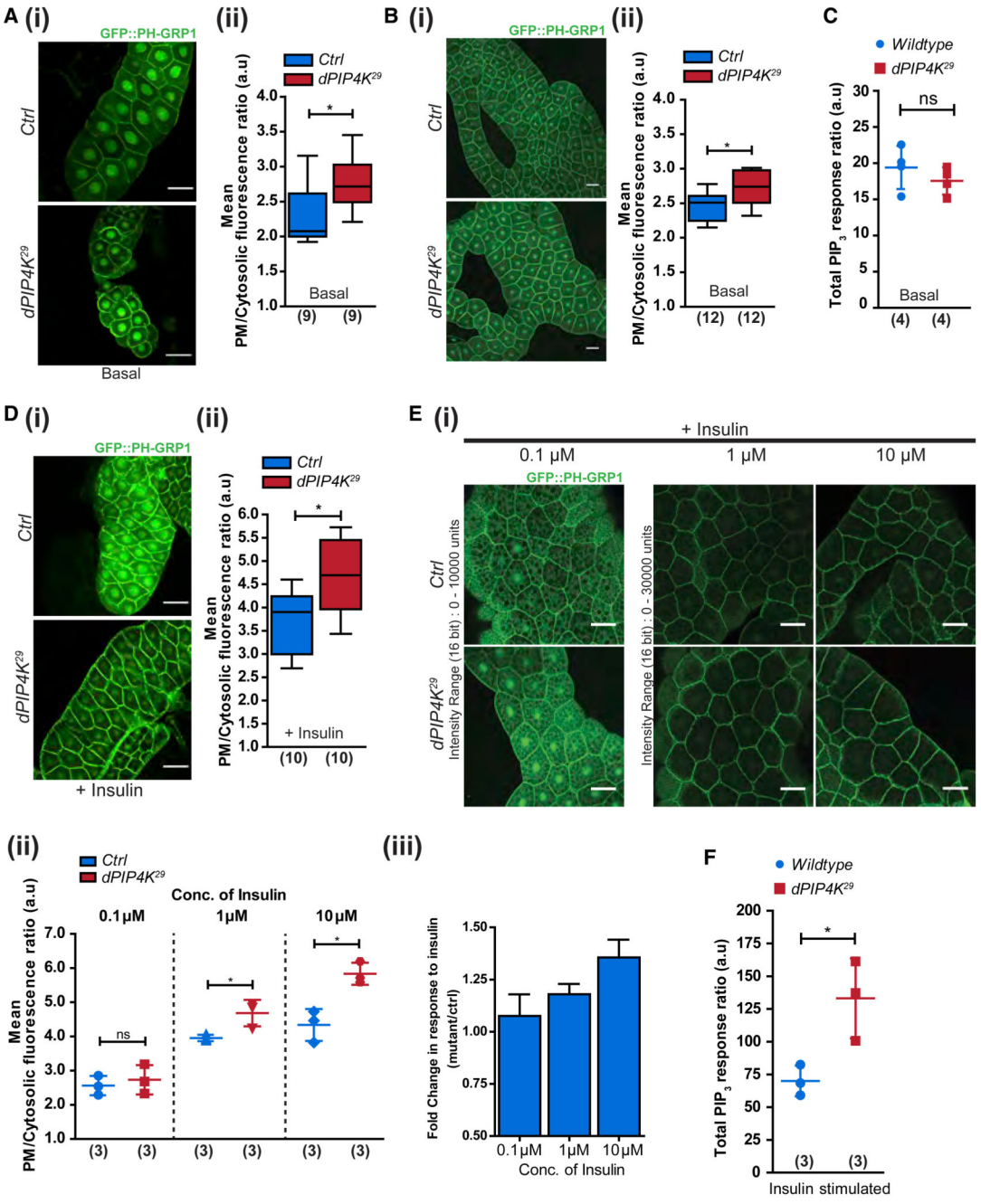

Figure 1. Loss of PIP4K Increases PIP_3 Levels

(A and B) Representative confocal images with the distribution and quantification of PIP_3 levels using GFP::PH-GRP1 probe in (Ai and Aii) larval salivary glands and (Bi and Bii) larval fat body. Scale bars: 50 µm in salivary gland images; 10 µm in fat body images.

(C) Total PIP_3 levels using LCMS in whole larval lipid extracts.

(D) Confocal z-projections depicting PIP_3 levels in (i and ii) insulin-stimulated (10 µM insulin, 10 min) salivary glands.

Europe PMC Funders Author Manuscripts

(E) Fat body lobes stimulated with 0.1, 1, and 10 μM insulin after 2-h starvation. Scale bars: 50 μm. (iii) Mean fold change in response to insulin (from data in ii).
(F) Total PIP_3 levels using LCMS in insulin-stimulated whole larval lipid extracts.
Boxplots with whiskers at minimum and maximum values, a line at the median, and scatterplots with mean ± SD are shown. Numbers in parentheses below the plots indicate the number of biological replicates. Statistical tests: (A, B, and D) Mann-Whitney test and (C, E, and F) Student's unpaired t test. *p value < 0.05. See also Figures S1 and S2.

Europe PMC Funders Author Manuscripts

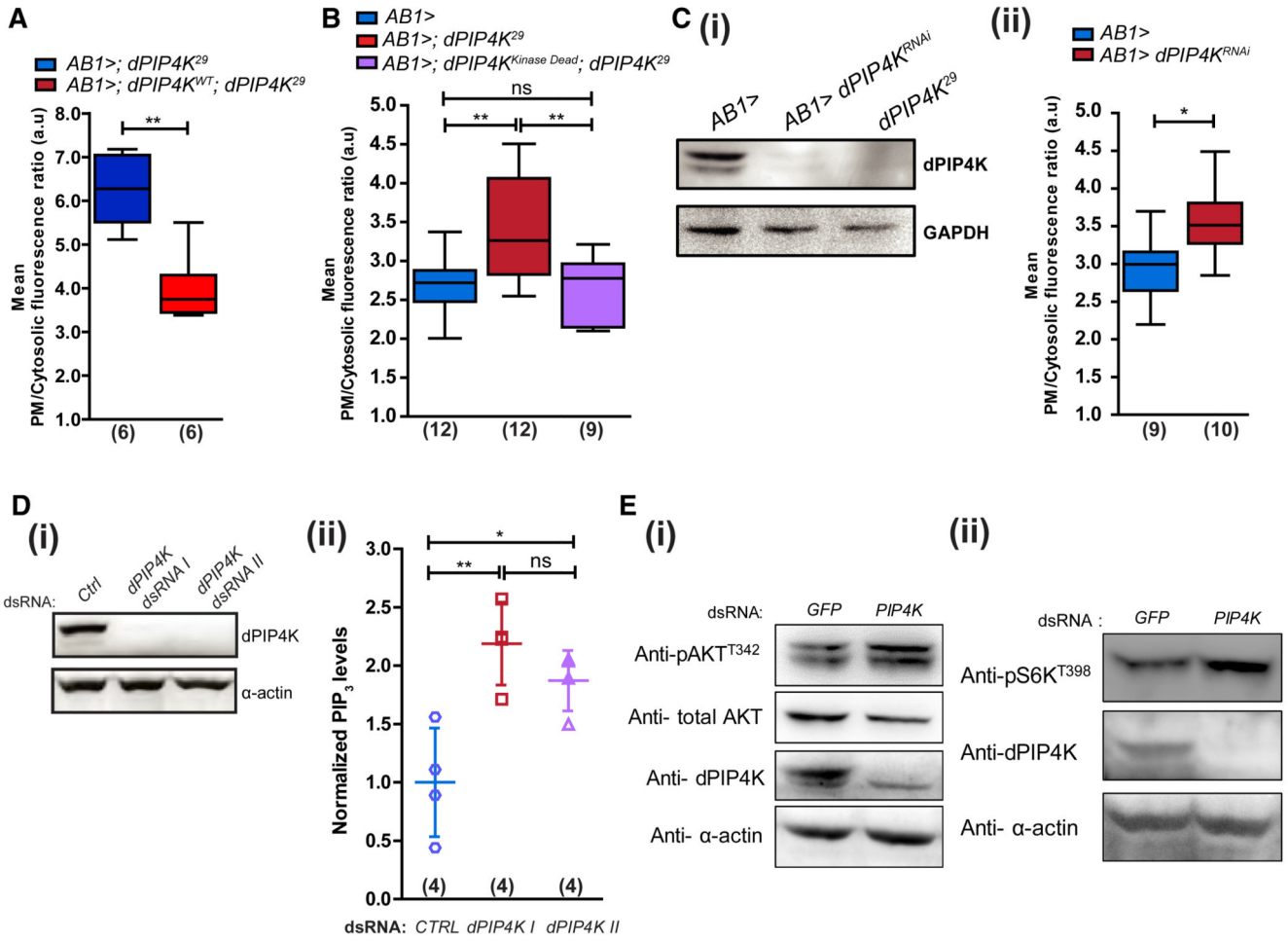

Figure 2. dPIP4K Cell-Autonomously Controls PIP_3 Levels

PIP_3 levels in salivary glands.

(A) Mutant and wild-type dPIP4K rescue.

(B) Control, mutant, and kinase-dead dPIP4K rescue.

(C) (i) Immunoblot (from wandering third instar larvae) showing salivary gland-specific depletion of dPIP4K (*dPIP4K^{RNAi}*). (ii) PIP_3 levels in control and *dPIP4K^{RNAi}* salivary glands.

(D) (i) Immunoblot for dPIP4K knockdown in $S2R^+$ cells with two different dsRNAs. (ii) Total PIP_3 using LCMS in whole cell lipid extracts of $S2R^+$ cells treated with indicated dsRNAs (data pooled from two experiments, a total of four biological replicates). Scatter plots with mean ± SD. Statistical test: one-way ANOVA with post hoc Tukey's multiple pairwise comparison. *p value < 0.05; **p value <0.01.

(E) Western blots for (i) $pAKT^{T342}$ and (ii) $pS6K^{T398}$ levels in control and dPIP4K knockdown cells.

See also Figure S2.

Europe PMC Funders Author Manuscripts

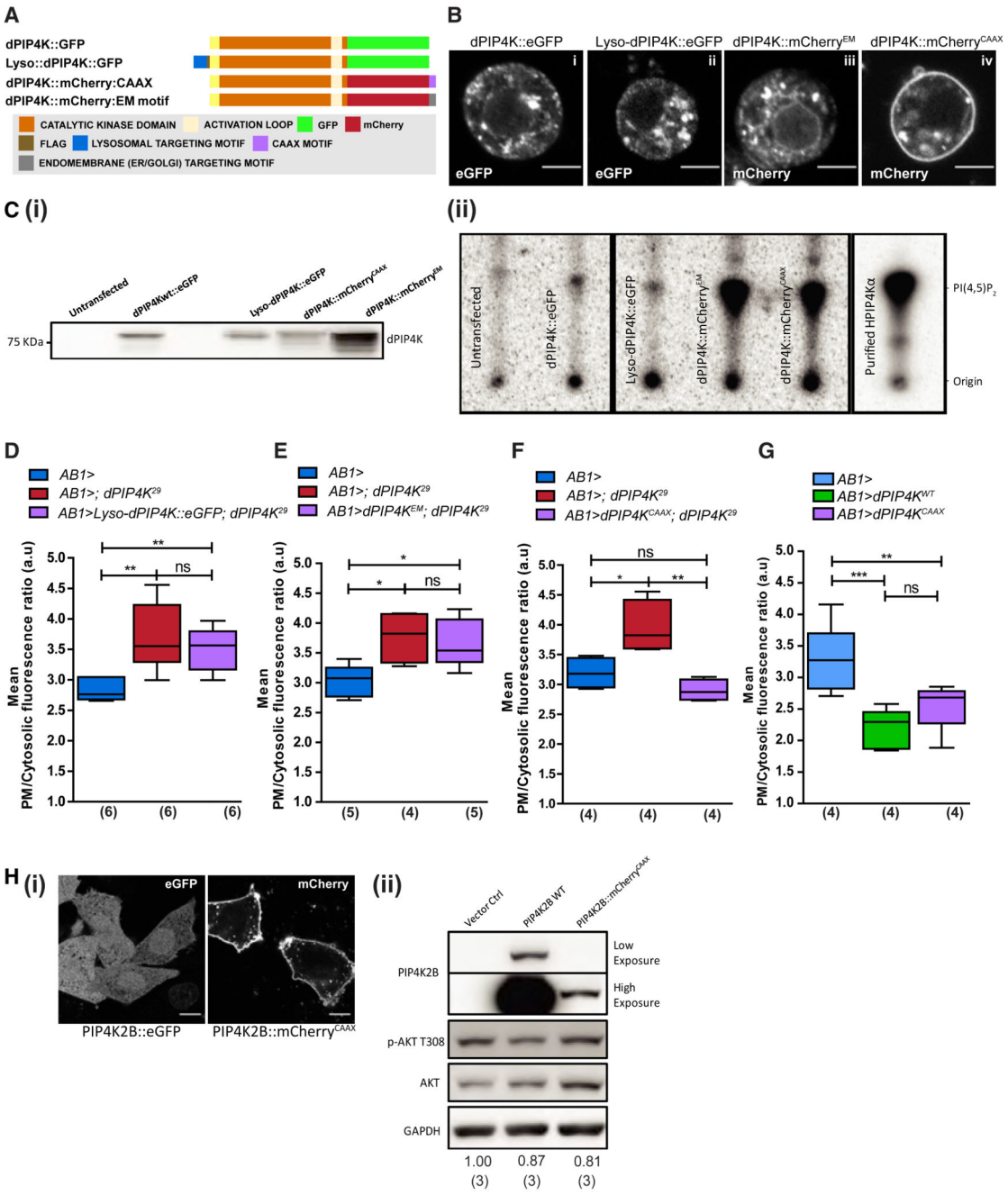

Figure 3. PIP4K Acts at the Plasma Membrane to Regulate Insulin-Stimulated PIP_3 Production

(A) Constructs targeting dPIP4K to different subcellular compartments.

(B) Confocal z-projections of S2R+ cells expressing (i) wild-type dPIP4K::eGFP, (ii) lysosome-targeted dPIP4K::GFP (Lyso-dPIP4K::eGFP), and dPIP4K::mCherry targeted to (iii) endomembranes (dPIP4K::mCherry^{EM-} ER, Golgi, and endo-lysosomal system) and (iv) plasma membrane (dPIP4K::mCherry^{CAAX}).

Europe PMC Funders Author Manuscripts

(C) (i) Immunoblots from S2R+ lysates expressing indicated *dPIP4K* constructs used in the *in vitro* assay. (ii) *In vitro* PIP-kinase assay for different *dPIP4K* constructs from S2R+ cell lysates.

(D–G) PIP_3 measurement using the PH-GFP-GRP1 probe in insulin-stimulated (10 μM) $dPIP4K^{29}$ salivary glands reconstituted with (D) Lyso-dPIP4K::eGFP, (E) dPIP4K::mCherry^{EM}, and (F) dPIP4K::mCherry^{CAAX}, and (G) overexpression of wild-type dPIP4K and dPIP4K::mCherry^{CAAX}.

(H) (i) Representative confocal z-projections of CHO-IR cells expressing GFP-PIP4K2B and PIP4K2B::mCherry-CAAX. Scale bars: 10 μm. (ii) Immunoblots for pAKT from insulin-stimulated (1 μM, 10 min) CHO-IR cells.

Numbers below the blots are mean pAKT/Tot-AKT ratios from three independent experiments. Boxplots with whiskers at minimum and maximum values and a line at the median are shown. Numbers in parentheses below the plots indicate the number of biological replicates. Statistical tests: (D–G) one-way ANOVA with post hoc Tukey's multiple pairwise comparison. *p value < 0.05; **p value < 0.01. See also Figures S3 and S4.

Europe PMC Funders Author Manuscripts

Europe PMC Funders Author Manuscripts

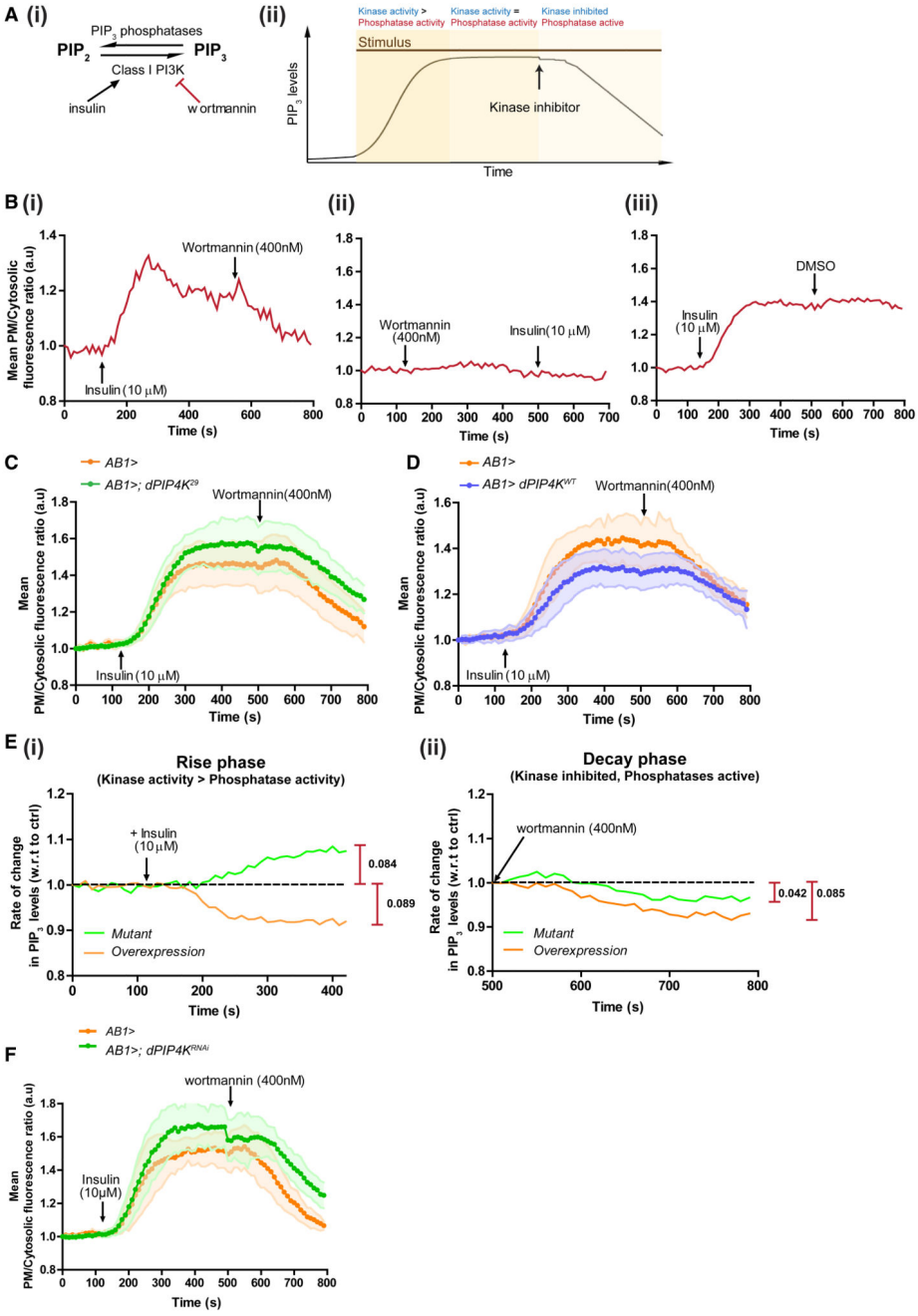

Figure 4. dPIP4K Alters PIP_3 Turnover by Limiting Class I PI3K Activity

(A) (i) Reactions influencing PIP_3 turnover at the plasma membrane. Insulin activates PI3K, and wortmannin irreversibly inhibits PI3K. (ii) Three phases in the live-imaging assay to follow PIP_3 dynamics.

(B) Single live-imaging traces of plasma membrane/cytosolic PIP_3 probe fluorescence ratio from salivary glands expressing GFP::PH-GRP1.

(C and D) Comparison of average live-imaging traces of PIP_3 probe fluorescence ratios in (C) control and *dPIP4K*^{29}, and (D) control and *dPIP4K* overexpression salivary glands (N =

7 imaging runs for all genotypes, minimum of about nine cells analyzed from each run). Error bars: SD. Controls were repeated as the two experiments were performed at different times.

(E) Normalized differences in instantaneous rate of change in fluorescence (ratio of test to that in controls); maximal difference is indicated alongside.

(F) PIP_3 levels in wild-type and dPIP4K-overexpressing salivary glands. Live salivary gland PIP_3 dynamics upon knockdown of dPIP4K.

See also Figure S5.

Europe PMC Funders Author Manuscripts

Europe PMC Funders Author Manuscripts

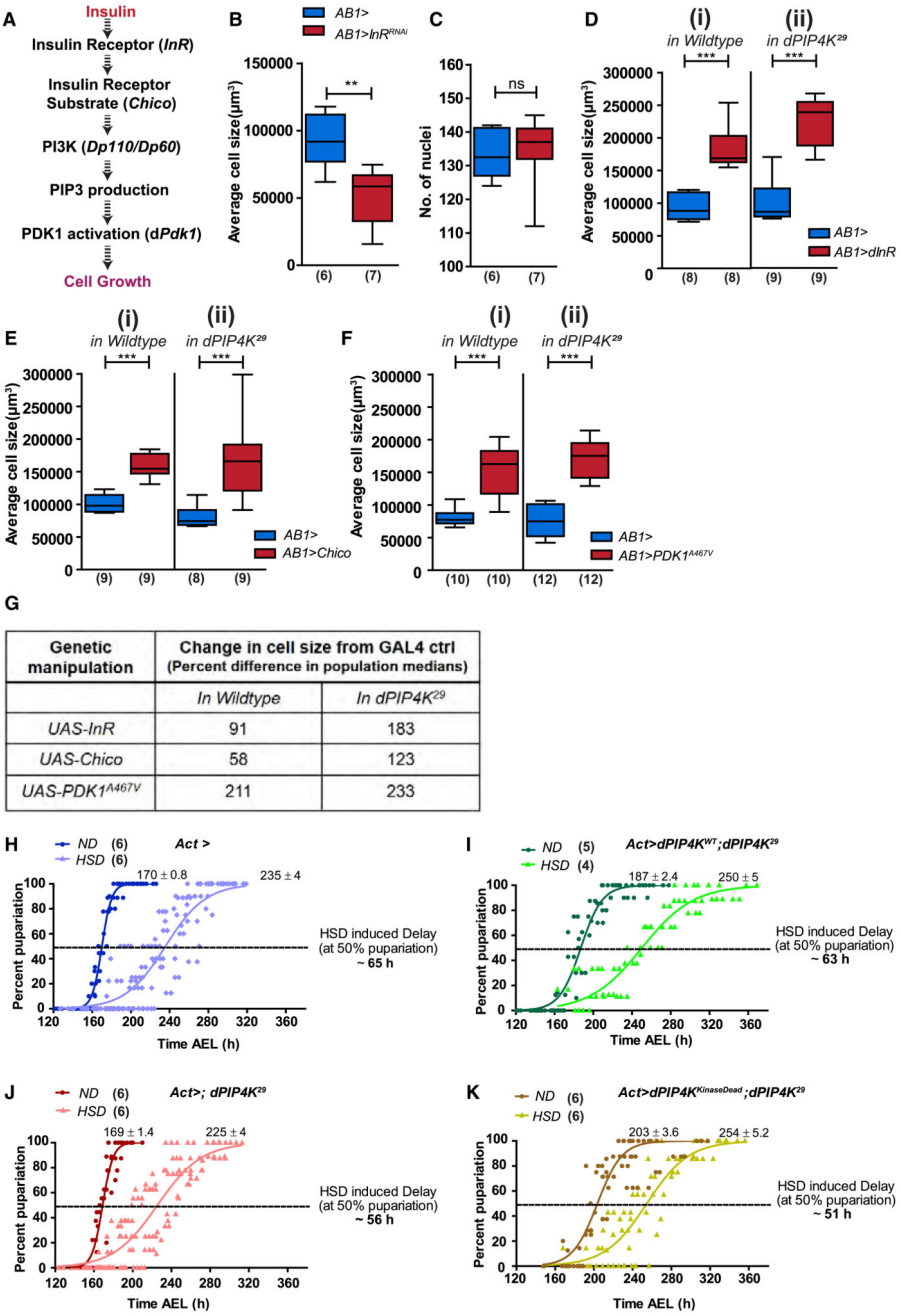

Genetic manipulation	Change in cell size from GAL4 ctrl (Percent difference in population medians)	
	In Wildtype	*In dPIP4K²⁹*
UAS-InR	91	183
UAS-Chico	58	123
UAS-PDK1^A467V	211	233

Figure 5. dPIP4K Interacts with Insulin Receptor Signaling *In Vivo* to Modulate Larval Physiology

(A) Components of insulin signaling cascade used in the study.

(B and C) Salivary gland (SG) cell size measurements (B) and quantification of the number of nuclei (C) upon knockdown of insulin receptor in salivary glands.

(D–G) SG cell size measurements in wild-type (*ROR*) and *dPIP4K²⁹* backgrounds upon (D) overexpression of dInR, (E) overexpression of Chico, (F) overexpression of PDK1^{A467V}, and (G) change in median SG cell sizes across different genetic manipulations.

(H–K) Percentage pupariation over time (after egg laying [AEL]) for genotypes - (H) Act>, (I) *Act>dPIP4K^{WT}; dPIP4K^{29}*, (J) *Act>; dPIP4K^{29}*, and (K) *Act>dPIP4K^{KinaseDead}; dPIP4K^{29}* on normal (ND) and high-sugar (HSD) diets. GraphPad Prism used to fit a variable slope curve for each genotype. Numbers indicate the time ± 95% confidence interval (CI) (h) at 50% pupariation. Boxplots with whiskers at minimum and maximum values and a line at the median are shown. Numbers in parentheses on the plots indicate number of biological replicates.

Statistical tests: (B–F) Mann-Whitney test. **p value < 0.01; ***p value < 0.001. See also Figure S6.

Europe PMC Funders Author Manuscripts

Europe PMC Funders Author Manuscripts

	Sample							
	Drosophila Larvae				S2R+ cells			
	Acyl species	PIP_3 Parent Ion	PIP_2 Parent Ion	Daughter Ion	Acyl species	PIP_3 Parent Ion	PIP_2 Parent Ion	Daughter Ion
MRM Transitions	32_1	1147.5	1039.5	549.5	30_1	1119.5	1011.5	521.5
	32_2	1145.5	1037.5	547.5	30_3	-	1007.5	517.5
	34_1	1175.5	1067.5	577.5	30_4	-	1005.5	515.5
	34_2	1173.5	1065.5	575.5	32_0	1149.5	1041.5	551.5
	34_3	1171.5	1063.5	573.5	32_1	1147.5	1039.5	549.5
	36_1	1203.5	1095.5	605.5	32_2	1145.5	1037.5	547.5
	36_2	1201.5	1093.5	603.5	32_3	-	1035.5	545.5
	36_3	1199.5	1091.5	601.5	34_0	1177.5	1069.5	579.5
	36_4	1197.5	1089.5	599.5	34_1	1175.5	1067.5	577.5
					34_2	1173.5	1065.5	575.5
					34_3	1171.5	1063.5	573.5
					34_4	1169.5	1061.5	571.5
					34_5	1167.5	1059.5	569.5
					36_0	-	1097.5	607.5
					36_1	-	1095.5	605.5
					36_2	1201.5	1093.5	603.5
					36_3	1199.5	1091.5	601.5
					36_4	1197.5	1089.5	599.5
					36_5	1195.5	1087.5	597.5

Europe PMC Funders Author Manuscripts

	Sample							
	Drosophila Larvae				S2R+ cells			
	Acyl species	PIP_3 Parent Ion	PIP_2 Parent Ion	Daughter Ion	Acyl species	PIP_3 Parent Ion	PIP_2 Parent Ion	Daughter Ion
					38_0	-	1125.5	635.5
					38_2	-	1121.5	631.5
					38_3	1227.5	1119.5	629.5
					38_4	1225.5	1117.5	627.5
					38_5	1223.5	1115.5	625.5
					37_4 ISD	1211.5	-	613.5